NAA-SR-4529
REACTORS-POWER
69 PAGES

FUEL BURNUP STUDIES FOR A 255 Mwe ADVANCED SODIUM GRAPHITE REACTOR

By
A. L. ARONSON

ATOMICS INTERNATIONAL
A DIVISION OF NORTH AMERICAN AVIATION, INC.
P.O. BOX 309 CANOGA PARK, CALIFORNIA

CONTRACT: AT(11-1)-GEN-8
ISSUED: JUNE 15, 1960

DISTRIBUTION

This report has been distributed according to the category "Reactors-Power" as given in "Standard Distribution Lists for Unclassified Scientific and Technical Reports" TID-4500 (15th Ed.), August 1, 1959. A total of 620 copies was printed.

CONTENTS

TABLES

FIGURES

FIGURES

ABSTRACT

Reactivity and fuel burnup studies were performed for a 255 Mwe sodium-graphite reactor of the advanced calandria core type. This reactor is briefly described. Initial criticality calculations and flux distributions were obtained, using two-group theory for enrichments between 2.0 at. % U^{235} and 4.0 at. % U^{235}. A four-group burnup study was performed for enrichments between 2.5 at. % U^{235} and 3.25 at. % U^{235}. Core lifetime, changes in isotopic fuel composition, variations in radial power distribution, and fuel cross sections are presented. Reactivity during core lifetime was assumed to be controlled by the presence of a homogeneous poison which simulated the effects of control rods. The results presented are useful in determining initial enrichment selection in fuel programming and fuel cost studies.

I. INTRODUCTION AND DESCRIPTION OF REACTOR

Advanced concepts in sodium-cooled graphite-moderated reactor design include a change from cores such as those of the Sodium Reactor Experiment and HNPF (with their individually canned, hexagonal blocks of graphite) to the calandria-core design incorporating uncanned, hexagonal blocks of graphite pierced by steel process-channels. These systems have been compared in detail, and the general advantages of the calandria design have been described.[1] These are two features, significant in the physics analysis, where the calandria differs from the canned moderator design. One feature is the smaller amount of structural material required in the core, resulting in a decrease in the nuclear poisoning effect. The other is the increased, average, moderator temperature, caused by the requirement that most of the heat generated in the graphite must be removed through the process tubes or the calandria shell. The high, average, moderator temperature affects the neutron cross-sections.

This report presents fuel-burnup studies and the associated physics analysis for a reactor of the calandria-core type. The reactor and system used as a basis for these studies are designed to produce 606 Mwt and 256 Mwe. A full description of this system is given elsewhere[2] and a summary of the details pertinent to this work appears below.

The graphite stack, including reflector, consists of uncanned, hexagonal, graphite logs 9.91 in. across the flats and 16 ft in length. They are located on a 10-in. triangular lattice spacing. The active height of the core is 12 ft, with a 2-ft-thick reflector above and below the core. Each graphite log in the core is pierced by a vertical process channel. There are 187 such channels, of which 168 are available for fuel, one for the neutron source and 18 for control and safety rods. The diameter of the stack if 16 ft. With a full reactor loading, the active core diameter is 12 ft, leaving a 2-ft-thick reflector in the radial direction.

The fuel element (Figure 1) consists of a cluster of 19 fuel rods made up of uranium carbide slugs, 0.50 in. in diameter, clad in stainless steel jackets 0.52-in. ID and with a wall thickness of 0.010 in. Sodium provides a thermal bond between the fuel slug and the cladding. The fuel cluster is surrounded by

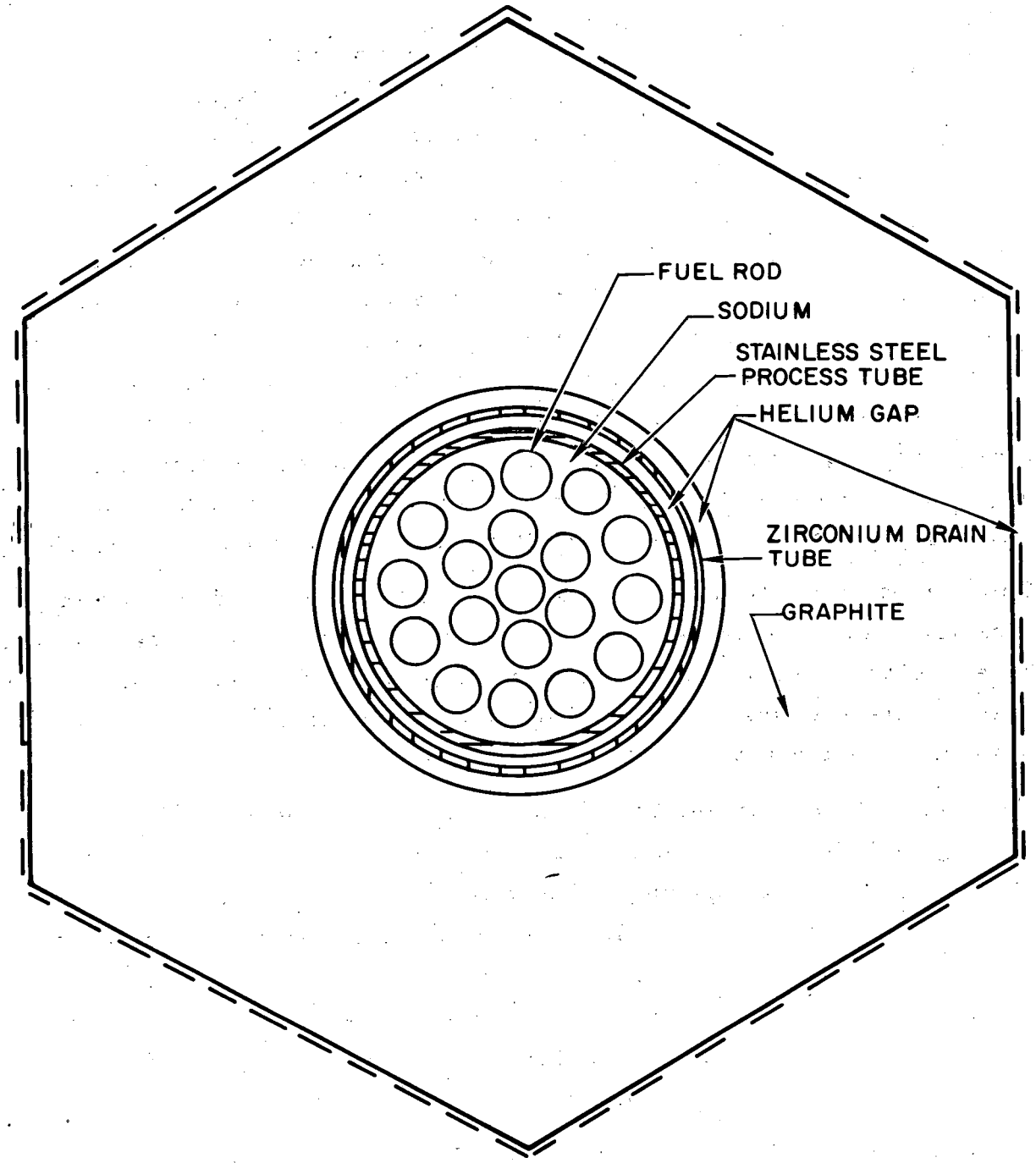

Figure 1. Fuel Cell in 255 Mwe ASGR

a stainless-steel process tube 3.330-in. ID with 0.020-in.-thick walls. The sodium coolant flows upward through the process tube in the space not occupied by the fuel rods. The process tube is located in a 3.530 in. diameter bore of the graphite log. It is surrounded by a zirconium drain tube 3.410-in. ID and 0.010 in. thick, with a helium gap of 0.020 in. between the process tube and the drain tube and a gap of 0.050 in. between the drain tube and the graphite.

In the calculational model, the interior of the channels reserved for source and control elements was treated as a void. The control rods and source were assumed to have been withdrawn. Only 150 fuel positions were used. The outermost 18 channels had graphite plugs inserted to fill the entire process tube. The effect of these plugs was to decrease the radius of the active core and increase the effective radial reflector thickness. The source channel was located at the center of the core with the control channels uniformly distributed throughout the rest of the core.

II. CRITICALITY CALCULATIONS

A. GEOMETRY AND CROSS SECTIONS

Initial criticality calculations were made using two-group theory. This was done for the condition of new fuel at full-power operation with equilibrium xenon and samarium present. Enrichments between 2.0 and 4.0 at. % U^{235} were considered. The average temperature in each material at full-power operation, along with the densities and thermal expansion coefficients used in these calculations, are given in Table I. From the dimensions at 20°C and the data in Table I, the dimensions and isotopic number densities at operating conditions were computed.

For the thermal group, a Maxwellian neutron spectrum was adopted with a neutron energy of 0.131 ev based on an average graphite temperature of 1250°C. Microscopic thermal cross-sections used are listed in Table II. The choice of these cross sections is discussed in the Appendix.

TABLE I

MATERIAL TEMPERATURES AND PHYSICAL CONSTANTS FOR 255 Mwe ASGR

Material	Average Temperature At Full-Power Operation (°C)	Density at 20°C (gm/cm^3)	Average Coefficient of Thermal Expansion/°C
Uranium Carbide	815	12.8	12.2×10^{-6} Linear
Graphite	1250	1.70	7.8×10^{-6} Linear
Sodium	490	0.945	2.66×10^{-4} Volume
Stainless Steel	490	7.905	17.3×10^{-6} Linear
Zirconium	682	6.507	6.3×10^{-6} Linear

B. CELL CALCULATIONS AND THERMAL GROUP CONSTANTS

The thermal microscopic cross-sections were flux and volume weighted in computing thermal group constants. This weighting was accomplished by the successive application of two separate cell calculations. The first calculation

TABLE II

NUCLEAR CONSTANTS FOR 255 Mwe ASGR
WITH 2.5 at. % U^{235} ENRICHMENT

Constant*	Core	Axial Reflector	Radial Reflector
Σ_{ri}	0.002384	0.003175	0.003522
Σa_1	0.001527	0.000117	0.000013
$\nu\Sigma f_1$	0.001115	-------	-------
D_1	1.2034	1.2412	1.1741
Σa_2	0.004929	0.000972	0.000197
$\nu\Sigma f_2$	0.007209	-------	-------
D_2	0.8831	0.9309	0.8511
L^2	179.182	960.0	4330.0
τ	309.88	381.01	332.30
β^2	0.000149	------	------
$\bar{\phi}_2$ (core)	1.415×10^{14}	neutrons/cm^2/sec	
$\bar{\phi}_2$ (Fuel)	6.60×10^{13}	neutrons/cm^2/sec	
$\bar{\phi}_1$ (core)	2.77×10^{14}	neutrons/cm^2/sec	

Fuel Loading:

Metric Tons of Uranium	16.09
K_g of U^{235}	397.0

*Reactor at full-power operation
Subscript 1 refers to fast group
Subscript 2 refers to thermal group

was made to obtain the average properties of a fuel cell (Figure 1); the second calculation was made to obtain the average properties of a unit cell typical of the whole core, with 150 fuel cells, 1 source, and 18 control rods (Figure 2). The steps involved in these calculations are described below.

In the first step, the fuel cell was broken into 3 cylindrical regions. The innermost of these regions contained all the materials (fuel, sodium, thermal

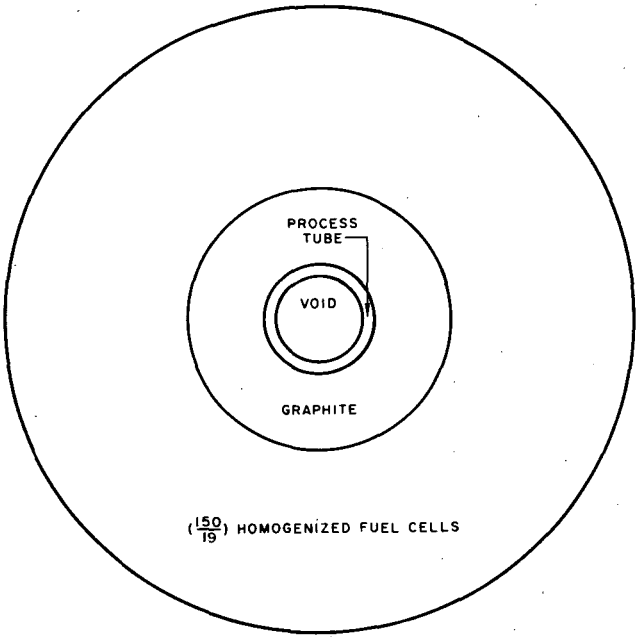

Figure 2. Typical Unit Cell in 255 Mwe ASGR

bond and coolant, stainless steel cladding) inside the process tube. The next region contained the stainless steel process tube, the zirconium drain tube, and the voids (helium) separating it from the process tube and the graphite. The outermost region (the graphite moderator log and the void between logs) was converted from a hexagon to a cylinder of equivalent area and inner radius. Each of these regions was individually homogenized. The fuel-material cross section in the innermost region was weighted with a disadvantage factor[3] to take into account the difference between the average flux within the fuel rod and the peak flux at the edge of the rod. Average constants were calculated for each region, and a cell thermal-flux distribution was obtained using the P_3 spherical harmonics approximation to the transport equation.[4] A representative flux distribution is shown in Figure 3. Average constants were computed for the fuel cell by flux and volume weighting the region cross sections so that

$$\sum = \frac{\sum_i \bar{\phi}_i V_i \sum_i}{\sum_i \bar{\phi}_i V_i} .$$

The symbols $\bar{\phi}_i$, V_i, and $\sum_i$ represent the average flux in region i, the volume fraction of region i, and the cross section of region i, respectively.

In the second step, a four-region cell was formed (Figure 2). The innermost region was a void corresponding to the inside of a control channel process tube with the control rod withdrawn. The next region consisted of the graphite log surrounding the process tube. The outermost region consisted of a material possessing the average properties of a fuel cell as computed above. The radius of the region was calculated to give the same ratio of fuel to control channels as existed in the core (150/19), since each control and source channel in the core

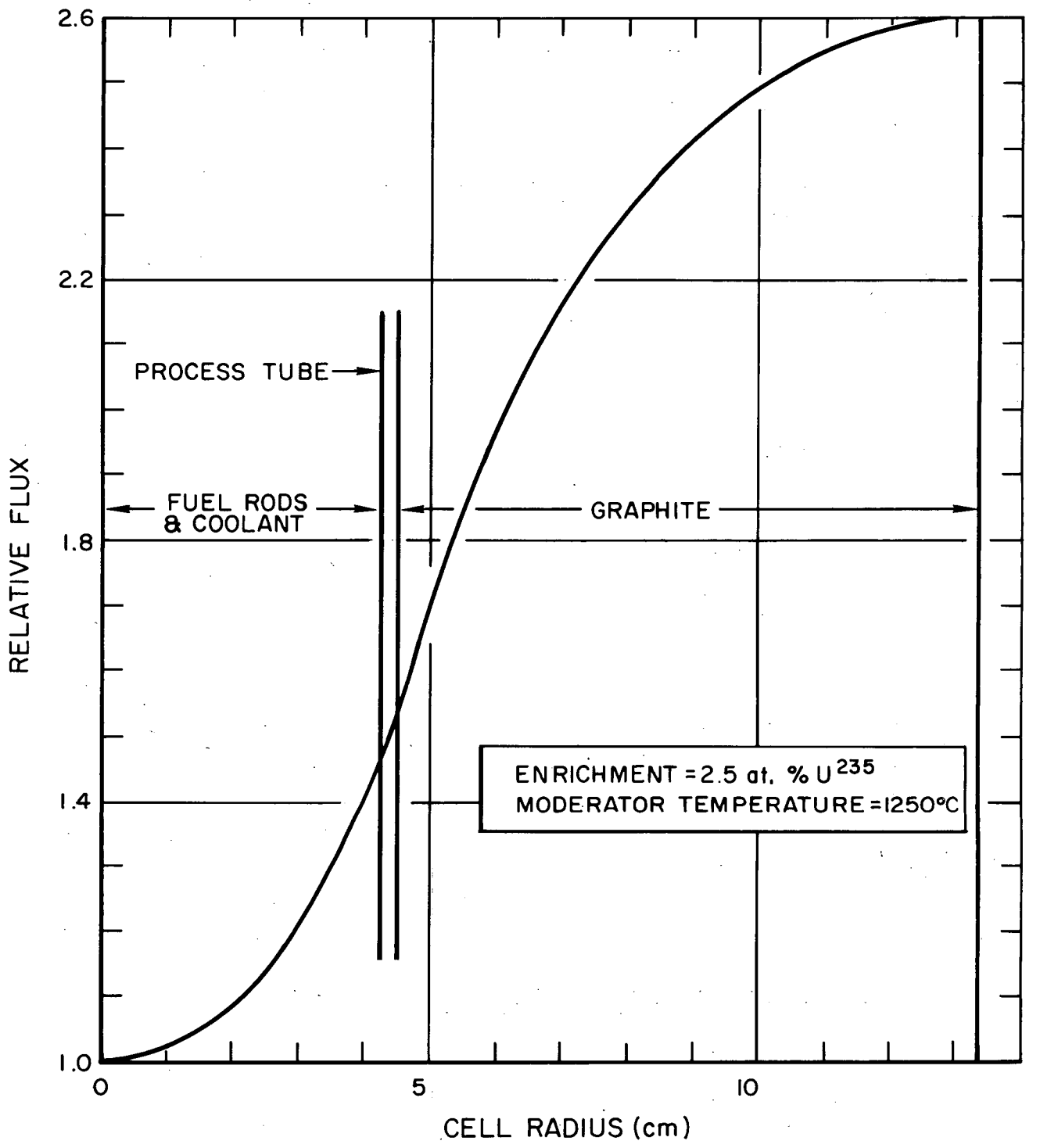

Figure 3. Thermal-Flux Distribution in a Fuel Cell of 255 Mwe ASGR

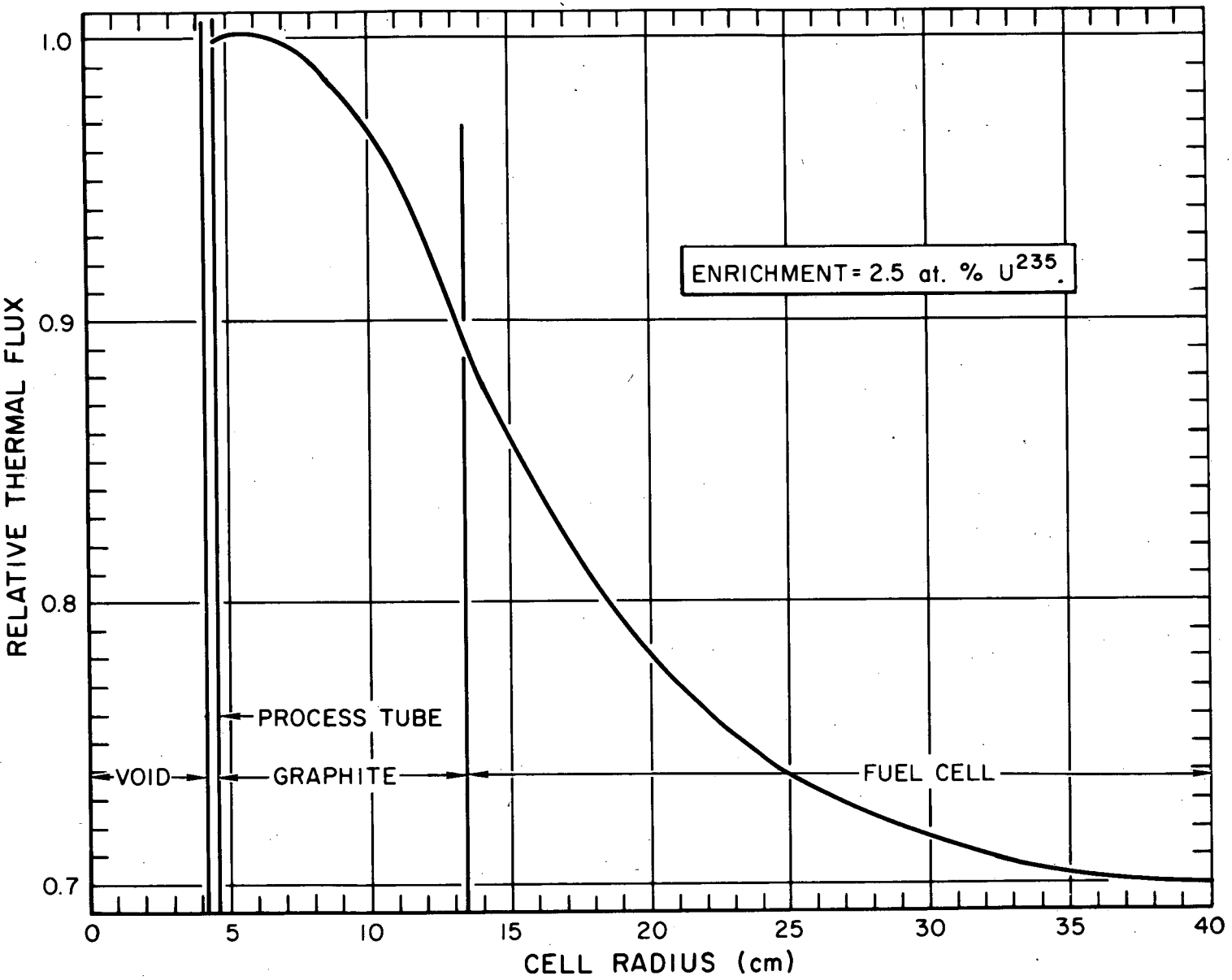

Figure 4. Thermal-Flux Distribution in a Unit Cell of 255 Mwe ASGR

was surrounded by an average of 150/19 fuel channels. A thermal-flux distribution for this cell was obtained from diffusion theory, using the WANDA Code.[5] A sample flux distribution for this unit cell is shown in Figure 4. Average region-fluxes were obtained, and the cross sections of the four regions were flux and volume weighted to give thermal constants for a unit cell typical of the core.

C. FAST-GROUP CONSTANTS

Fast-group constants were obtained using the MUFT-4 code.[6] The low-energy cut-off for the fast group was 0.625 ev. A flat spatial distribution of fast flux in the lattice cell was assumed, except in the resonance region. A self-shielding correction was made for resonance absorption in U^{238}. In order to obtain the surface-to-mass ratio for this correction, the model commonly used for multi-rod fuel clusters in sodium-graphite reactors was followed,[7] and the surface was taken as that of a taut rubber band surrounding the fuel cluster. A Doppler broadening correction was made for an average operating fuel temperature of 815°C, using a value of $\alpha = 1.5 \times 10^{-4}/°C$.

D. REFLECTORS

The radial reflector consists of two regions. The inner region contains the 18 unused fuel channels with dummy graphite plugs inside the process tube. This region was smeared over an annulus between the core and the blanket proper — a 2-ft thickness of solid graphite. Corrections were made for thermal expansion, the two regions homogenized, and the average, radial, reflector thermal-constants calculated.

The top and bottom reflectors have the same geometry. Each channel in the reflector region was taken as a vertical extension of the core channel without fuel. The sodium, zirconium, and stainless steel were weighted with a thermal-flux disadvantage factor of 0.9 (compared to 1.0 for the graphite), to allow for flux depression in the process tube. The various materials were homogenized to obtain axial reflector thermal constants. Fast-group constants, for both axial and radial reflectors, were obtained using the MUFT-4 code.[6]

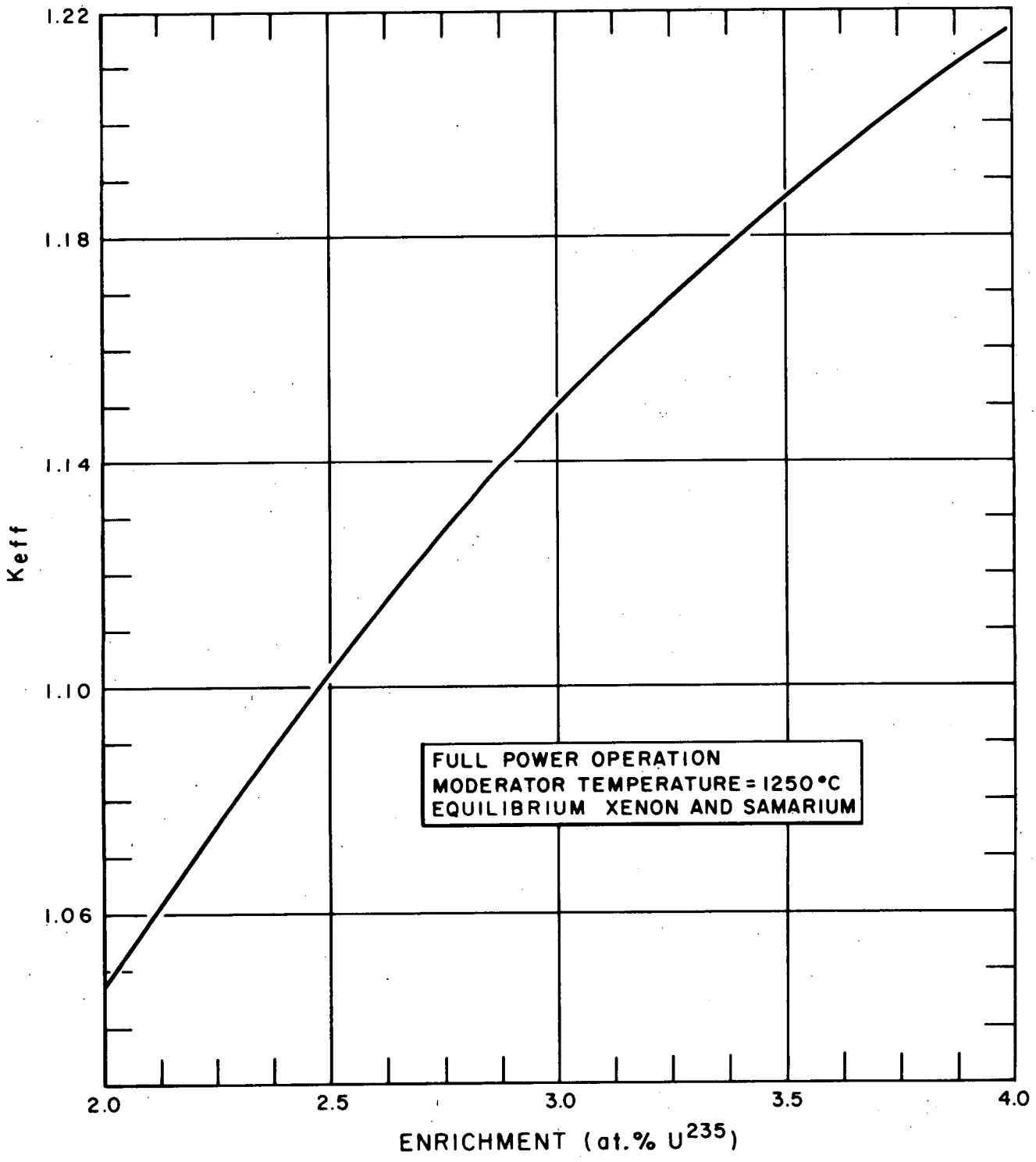

Figure 5. Variation of k_{eff} with Initial Enrichment

E. CRITICALITY AND FLUX DISTRIBUTION

From the dimensions and group constants for the reflector at operating temperatures, the axial reflector savings were initially estimated from a one-group expression.[8] An axial geometric buckling was computed; using this value for the transverse buckling, together with the two-group constants previously computed, the diffusion equation was solved by cylindrical geometry using the WANDA Code.[5] The solution of the diffusion equation was used to obtain the radial buckling which was used as the input transverse buckling for WANDA in two-region slab geometry. This procedure was repeated until radial and axial calculations converged to the same value for k_{eff}, at which point the values of radial and axial buckling for two successive calculations agreed. One iteration was sufficient when the initial estimate of reflector savings was accurate.

The value of effective multiplication was determined in the same way for values of initial enrichment between 2.0 and 4.0 at. % U^{235}, with the reactor at operating temperatures and with equilibrium xenon and samarium present. These values are shown in Figure 5. For the representative case of 2.5 at. % U^{235} enrichment, the two-group flux distributions in the radial and axial directions are shown in Figures 6 and 7. The lattice constants for this case are displayed in Table III; the neutron balance is shown in Table IV.

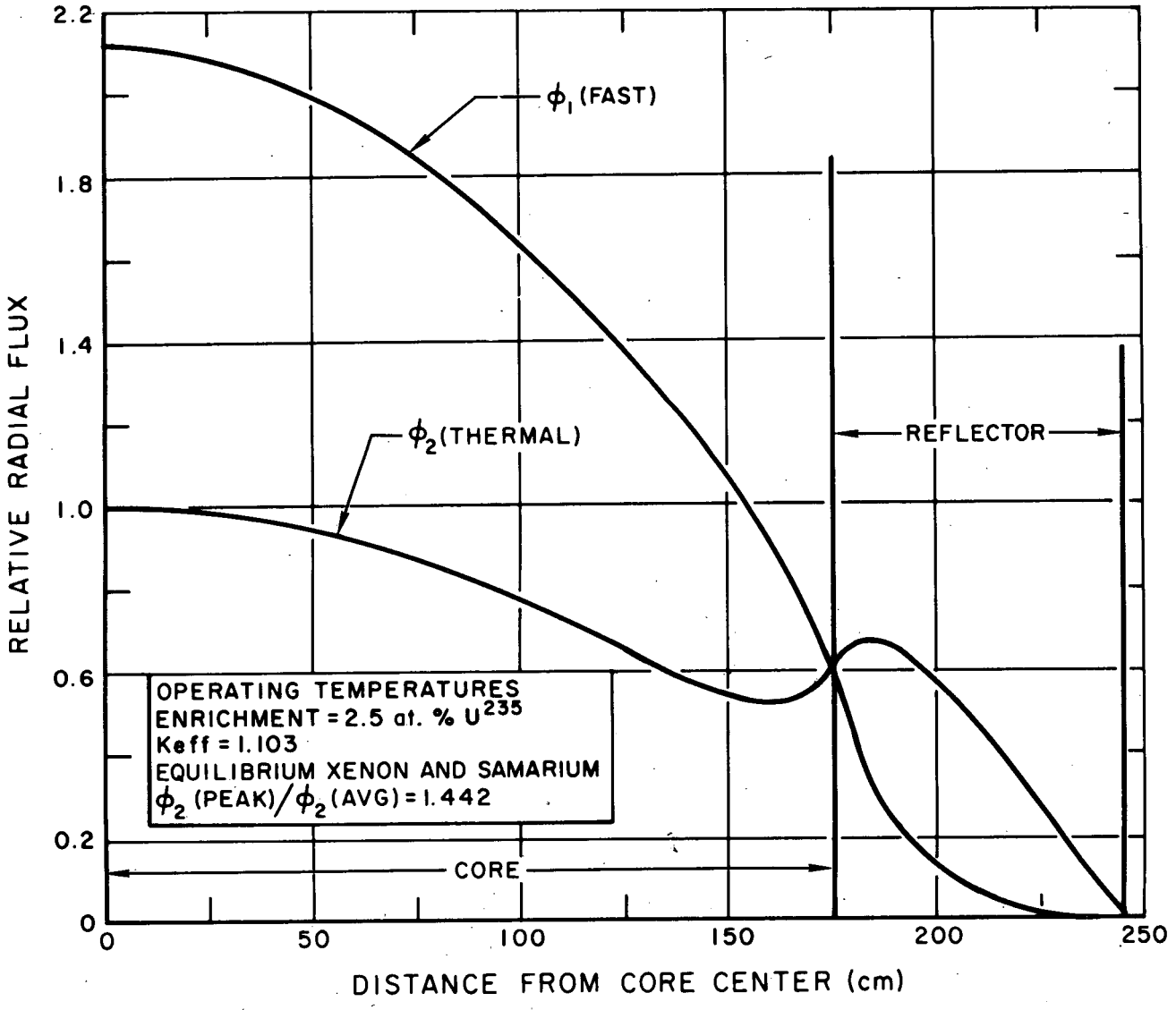

Figure 6. Two-Group Radial Flux Distribution in 255 Mwe ASGR

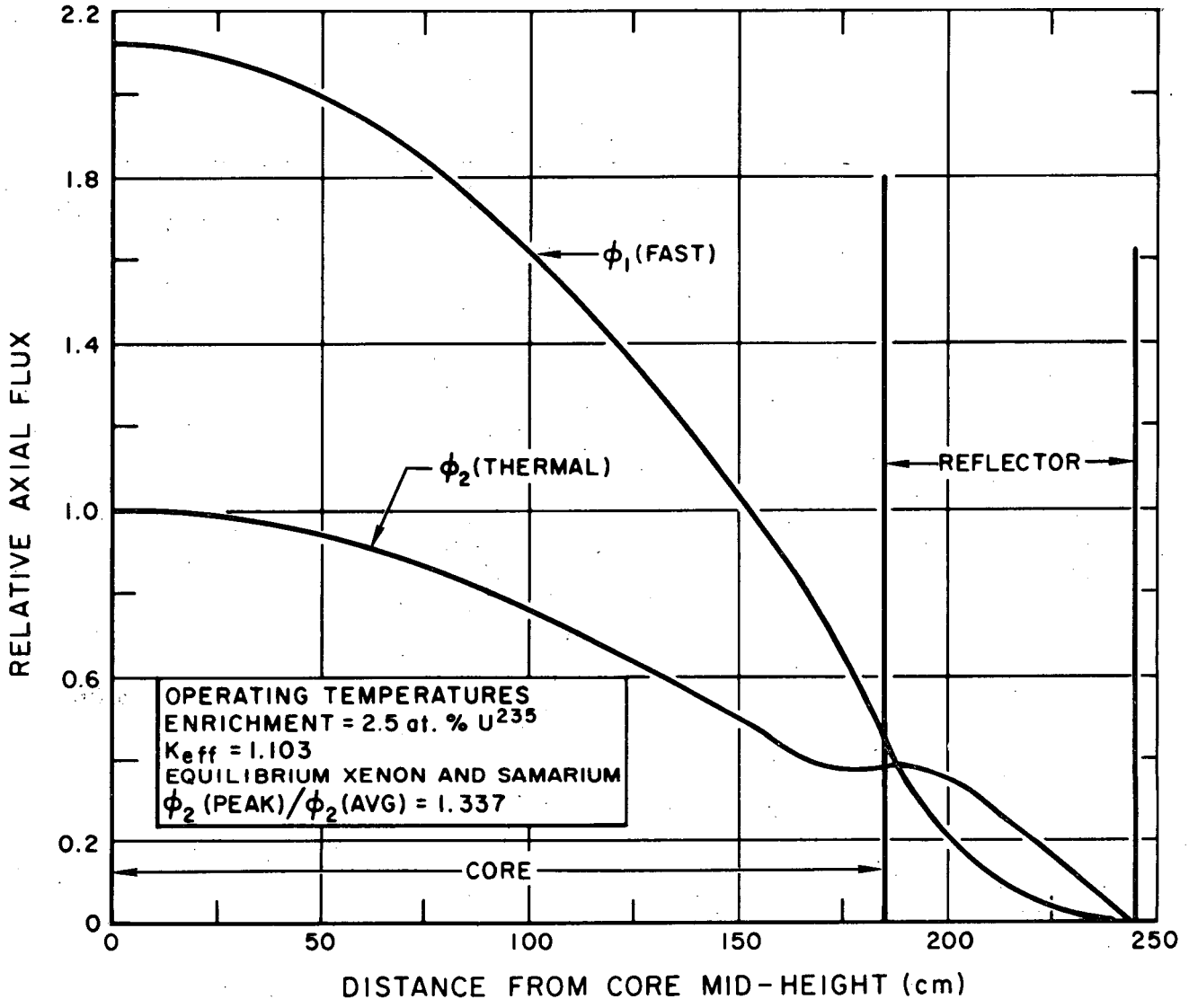

Figure 7. Two-Group Axial Flux Distribution in 255 Mwe ASGR

TABLE III

MICROSCOPIC THERMAL CROSS SECTIONS

Element	σ_s (barns)	$\overline{\sigma_a}^*$ (barns)	$\overline{\sigma_f}^*$ (barns)	ν
Graphite	4.8	0.0021		
Carbon	4.8	0.0013		
Stainless steel	9.76	1.1432		
Sodium	4.0	0.1944		
Zirconium	8.0	0.0836		
Uranium - 235	10.0	253.0	207.0	2.47
Uranium - 236	8.0	2.7219		
Uranium - 238	8.3	1.0538		
Plutonium - 239	9.6	1640.0	986.0	2.90
Plutonium - 240	9.6	180.6		
Plutonium - 241	9.6	1100.3	806.1	3.06
Xenon - 135		0.895×10^{6}		
Samarium - 149		2.52×10^{4}		
Average fission product pair		25.0		

*Maxwell Average at 0.131 ev.

TABLE IV

NEUTRON BALANCE FOR 255 Mwe ASGR WITH
2.5 at. % U^{235} ENRICHMENT

Fast Group	Neutrons Absorbed		Neutrons Produced
Graphite	0.1792		
Zirconium	0.0467		
Stainless steel	1.2435		
Sodium	0.5843		
U^{238} (Capture)	20.4681		
U^{238} (Fission)	1.6393		4.3597
U^{235} (Capture)	3.8695		
U^{235} (Fission)	9.2981		22.9012
Total absorbed fast		37.3287	
Leakage fast		4.3853	
Neutrons thermalized*		58.2860	
Thermal Group			
Graphite	1.6063		
Zirconium	0.0317		
Stainless steel	3.3013		
Sodium	1.0684		
U^{238} (Capture)	5.8541		
U^{235} (Capture)	6.5443		
U^{235} (Fission)	29.4490		72.7391
Xenon and samarium	1.8807		
Control rods	7.2220		
Total absorbed thermal		56.9580	
Leakage thermal		1.3282	
TOTAL		100.0000	100.0000

BASIS: Reactor at full-power operation
k_{eff} = 1.103 without control rods

Neutrons thermalized = total fission neutrons produced in previous generation — less fast neutrons lost due to absorption or fast leakage.

III. FUEL DEPLETION CALCULATIONS

A. GENERAL COMMENTS ON THE CANDLE CODE [11]

Fuel depletion studies were done (using the "CANDLE" Code) on the IBM-709 digital computer. "CANDLE" combines a one-dimensional solution of the diffusion equation with burnup equations for the change of concentration of isotopes in the uranium fuel system. It has a four-group structure, one thermal group and three fast groups. The group structure used is shown in Table V. The calculations were performed using cylindrical geometry.

TABLE V

CANDLE GROUP STRUCTURE

Group	Energy Range
1	10 - 0.825 Mev
2	825 - 5.53 kev
3	5530 - 0.625 ev
4	Less than 0.625 ev

Material isotopic number densities were uniform throughout the core at the beginning of operating history. Control-rod effects were simulated through the presence of a homogeneous poison in the core. The poison concentration was decreased as burnup proceeded in order to keep the core just critical. The poison was taken principally as a thermal poison, with a value in the 3rd (epithermal) group equal to 10% of the thermal value. This estimate was made to take into account expected epithermal effects of control rod materials.

The average core exposure was related to time by the relation

$$t = \overline{E} \times \frac{M}{P} \quad ,$$

where

t = time (days)

$\bar{E}$ = average core exposure $\frac{\text{megawatt-days}}{\text{metric ton of uranium}}$ (Mwd/MTU)

M = mass of uranium (metric tons) = 16.09 for core

P = power (Mw) = 606 per core

1000 $\frac{\text{Mwd}}{\text{MTU}}$ average core exposure = 26.6 days at full-power operation.

B. PREPARATION OF SELECTED INPUT

1. Thermal-Flux Disadvantage Factors

The variation of thermal flux within the lattice cell was taken into account through the use of "g" factors (thermal-flux disadvantage factors), defined for each material, M, as

$$g_M = \frac{\bar{\phi}_M}{\bar{\phi}_{cell}} .$$

As a first step in the selection of suitable g factors, the relative thermal flux in each material, as a function of fuel-absorption cross section, was obtained from the cell calculations previously performed. For the fuel cell, the ratio of the average flux in each region to the average flux in the cell was taken as

$$g_i = \frac{\bar{\phi}_i}{\sum_i \bar{\phi}_i V_i / \sum_i V_i} .$$

The same procedure was used for the unit cell. The product of the average flux in a region and the fraction of a material, M, that occurred in that region were summed over all the regions where material M occurred to give the average flux in that material.

An example to illustrate this procedure will be given for graphite in the core with a fuel enrichment of 2.5 at. % U^{235}. The ratio of the average flux in

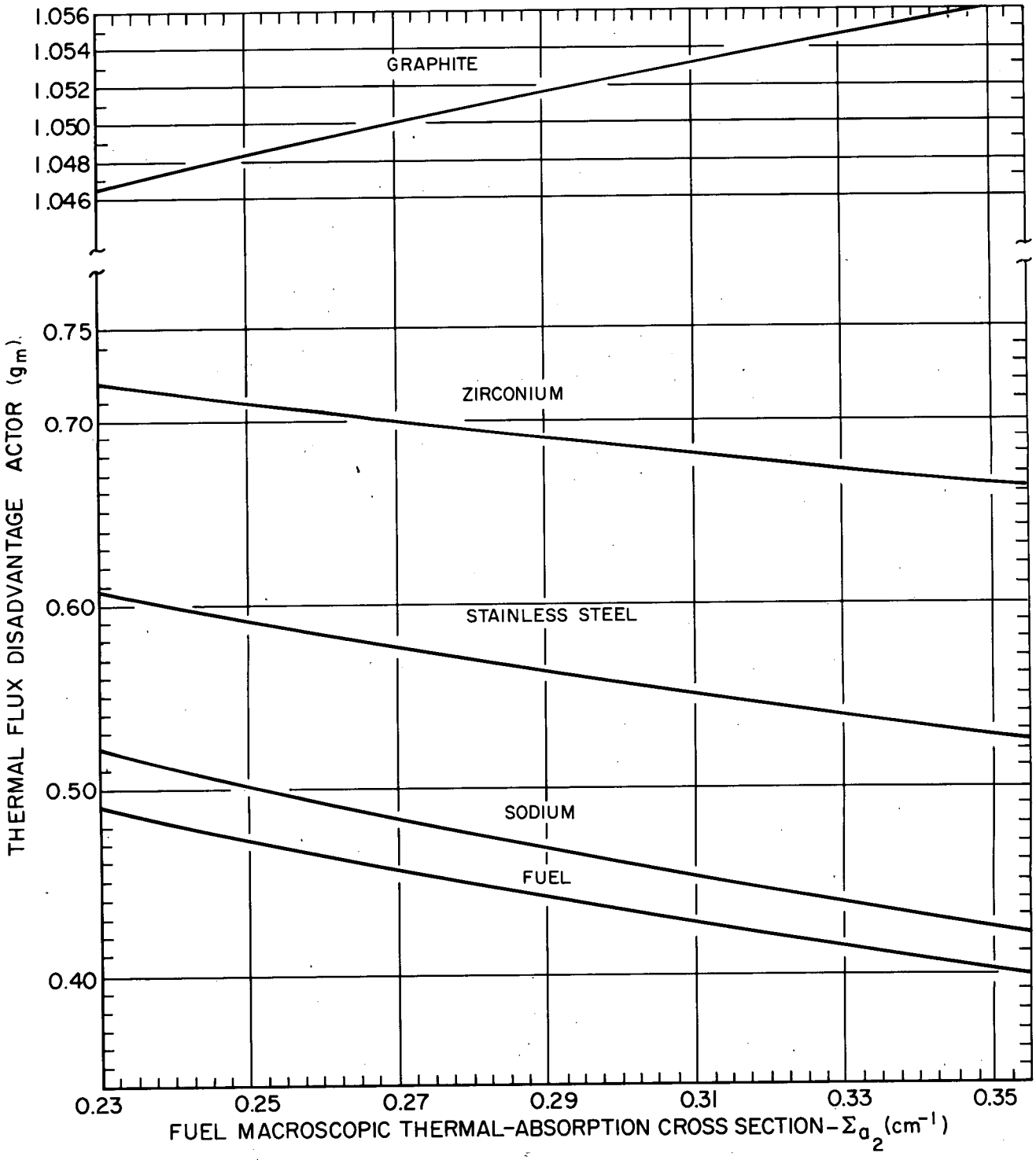

Figure 8. Variation of Thermal-Flux Disadvantage Factor (g_M) with Fuel-Absorption Cross Section in 255 Mwe ASGR

the outermost region of the fuel cell to the average flux in the whole fuel cell is 1.0550. The ratio of the average flux in the outermost region of a unit cell (the homogenized fuel cell) to the average flux in the whole unit cell is 0.9663. The ratio of the average flux in the graphite logs of the fuel channel to the average flux in the unit cell is, therefore, 1.0550 x 0.9663. Of the 169 graphite logs in the reactor, 150 logs surround fuel channels. The ratio of the average flux in the graphite log of a control channel to the average flux in the unit cell is 1.2599 (with the control rod withdrawn). There are 19 such channels in the core. Hence the ratio of the average flux in the graphite to the average flux in the unit cell is given as

$$g_{Graphite} = (1.0550 \times 0.9663) \times \left(\frac{150}{169}\right) + 1.2599 \times \left(\frac{19}{169}\right) = 1.0465 \quad .$$

The variation of g_M with initial (hot-clean) fuel absorption cross section is shown in Figure 8.

As fuel burnup proceeds, there is a variation in macroscopic fuel-absorption cross sections. Xenon and samarium increase to equilibrium concentrations in a short time and are followed by the gradual accumulation of low cross-section fission products. U^{235} become depleted and the various plutonium isotopes begin to build up. The net result of these changes is an increase in fuel-absorption cross section and a variation in the thermal-flux distribution in the lattice cell. The extent of this change, for a given lattice, is a function of the initial enrichment and the neutron temperature. For the narrow range of enrichments considered in this report, the effect of initial enrichment on percentage change in fuel-absorption cross section with time is small. The validity of this assumption can be confirmed by an examination of Figures 17-A, 17-B, 17-C, and 17-D in the results presented in Section IV.

A value of g_M was designed so that, properly averaged, it would give the same predicted core-operating lifetime as would be obtained by using a continuously varying value. First, the obtainable operational lifetime for a specified enrichment was estimated. The ratio of the average fuel cross-section over the operational lifetime to the initial value was then estimated. The accuracy of these estimates was checked against the results of the study and revised when

necessary. Since the initial hot-clean fuel absorption was known, the average value of the cross-section was computed, and the average value of g_M was obtained from Figure 8. Use of the g_M factors averaged over the operational life of the core gave an initial value of k_{eff} approximately 1% lower than that predicted by the use of g_M factors for the condition with only equilibrium xenon and samarium present. It has, however, a more accurate value over the entire life of the core. Since, for a core with an initially uniform fuel loading, the appropriate g_M factor at any subsequent time in the operating history is a function of position in the core, and since the more highly exposed elements at the center of the core have different g_M factors than those at the periphery, it was considered sufficiently accurate to approximate the changes with an average value.

2. Fast-Group Cross Sections

The three fast-group cross sections were based on MUFT-4. Iron and zirconium cross sections include recent resonance-integral data. Cross sections for U^{238} include the effects of self-shielding input to MUFT-4, to take into account a resonance integral appropriate to the uranium carbide fuel. Removal and transport cross sections were all assigned to graphite, since the MUFT-4 printout does not show contributions from individual elements to macroscopic removal cross-sections and diffusion coefficient. In order to obtain plutonium absorption and fission cross sections averaged over an appropriate flux spectrum, plutonium was included in some of the MUFT-4 calculations in a quantity to correspond to its average concentration over the operational life of the core. For Pu^{240}, a self-shielding factor (also based on an average concentration over the core operating lifetime) was included for the 1.055 ev resonance.

3. Resonance-Fitting Scheme

The third group (epithermal) required special treatment of some constants because of the CANDLE resonance-fitting arrangement. CANDLE treats the third-group macroscopic removal cross section as a function of (1) the product of the microscopic removal cross section and the number density of the corresponding isotope, (2) the smooth and resonance absorption in U^{238}, and (3) the smooth absorption in other materials. The third-group removal cross section is decreased by the buildup of plutonium isotopes and fission products with increasing fuel exposure. The value of the third-group microscopic removal cross section

σ_r^3 was chosen to make the third-group macroscopic removal cross section in CANDLE agree with that given by MUFT-4 at the beginning of the operating lifetime of the core.

An interrelated quantity is the resonance absorption in U^{238}. A smooth absorption cross section is stored on the library tape, but resonance absorption is provided for through the quantity P_{r3}^{28} where

$$P_{r3}^{28} = \frac{\sum_r^3 + \sum_{aS}^{28,3}}{\sum_r^3 + \sum_{aS}^{28,3} + \sum_{ar}^{28,3}} ,$$

or

$$\sum_{ar}^{28,3} = \left(\frac{1-P_{r3}^{28}}{P_{r3}^{28}} \right) \left(\sum_r^3 + \sum_{aS}^{28,3} \right) ,$$

where

$\sum_r^3$ = cross section for removal from 3rd group

$\sum_{aS}^{28,3}$ = cross section for smooth absorption in U^{238} in 3rd group

$\sum_{ar}^{28,3}$ = cross section for resonance absorption in U^{238} 3rd group.

The quantity P_{r3}^{28} is constant throughout the operating lifetime of the core. It was calculated from the MUFT-4 output in such a way that the value of $\sum_{ar}^{28,3}$ at the beginning of core life, as calculated by CANDLE, agreed with that given by MUFT-4.

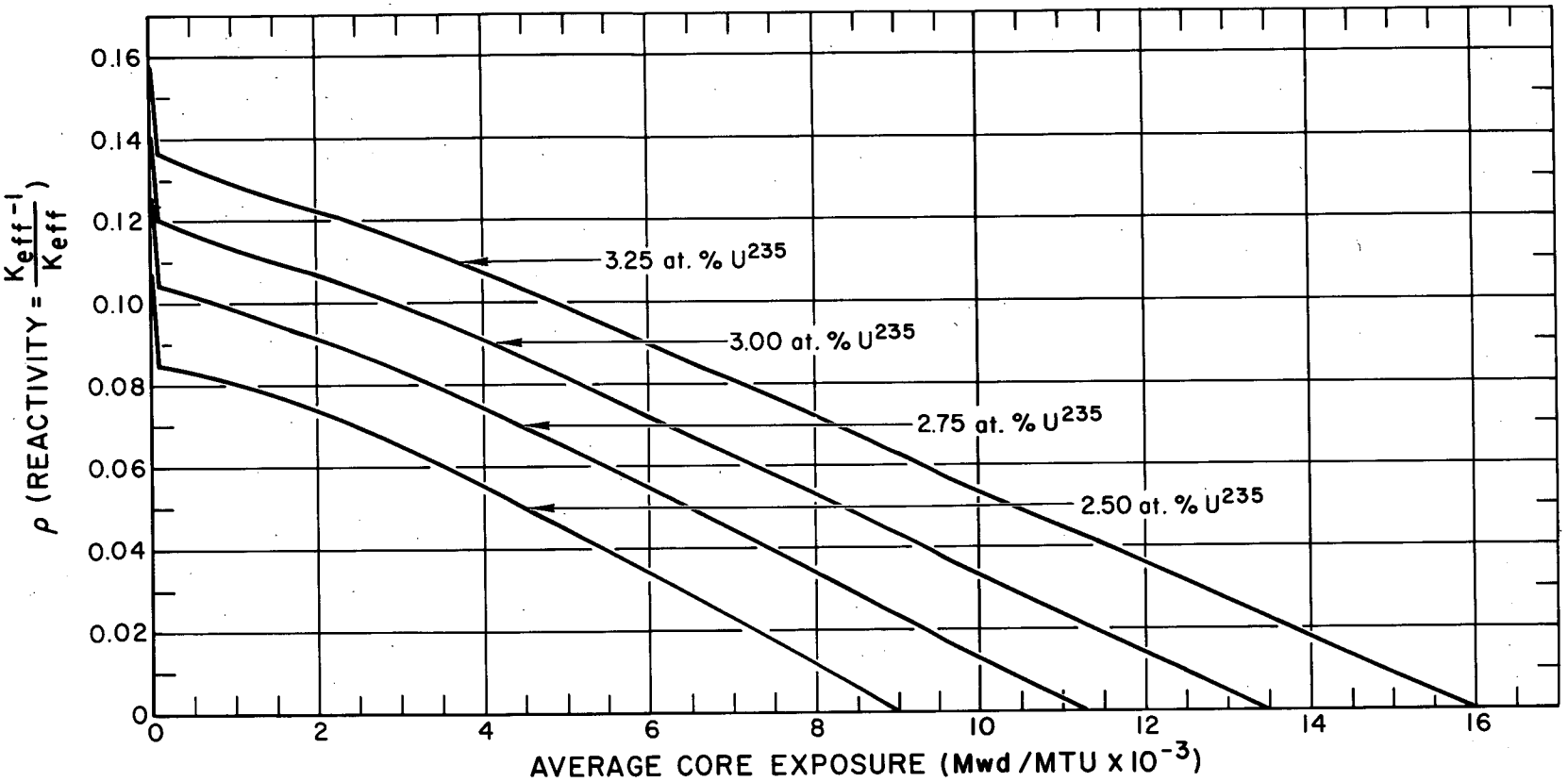

Figure 9. Variation of Reactivity with Burnup in 255 Mwe ASGR

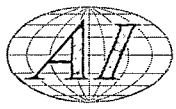

IV. PRESENTATION AND DISCUSSION OF RESULTS

A. REACTIVITY AND CONVERSION RATIO

The results of the burnup studies are presented graphically in Figures 9 through 18. Four cases were studied, with enrichments of 2.5 at. % U^{235}, 2.75 at. % U^{235}, 3.0 at. % U^{235}, and 3.25 at. % U^{235}. The interpretation and use of these results is discussed below.

Figure 9 shows the variation of reactivity, ρ, where $\rho = (k_{eff}-1)/k_{eff}$, available at any time if the control rods were withdrawn, as a function of average core exposure $\overline{E}$. The sharp initial decline in reactivity is associated with the buildup of an equilibrium concentration of the high cross-section fission-produce Xe^{135}. Thereafter, the decline in reactivity is slow, for a time, and gradually becomes steeper. This effect of slow initial decline in reactivity (after the buildup of equilibrium Xe^{135} concentration), followed by a more rapid subsequent falloff, can be seen most clearly in the 2.5 at. % U^{235} enrichment case and less markedly as enrichment increases. This phenomenon is to be expected; because of the decrease in conversion ratio with increasing enrichment, reactors fueled with natural uranium exhibit an actual initial rise in reactivity followed by a subsequent decline. For fuels with increasing enrichment, the initial rise becomes less marked because of smaller conversion ratios, and finally the decline in reactivity becomes monotonic. The slow initial falloff in reactivity, followed by a more rapid decline, does persist but becomes less marked as enrichment increases.

The curves of Figure 9 can be used to predict the reactivity at any time subsequent to core startup. The enrichments considered (2.5 at. % U^{235} to 3.25 at. % U^{235}) included the range of practical interest (Figure 5). Enrichments of less than 2.5 at. % U^{235} gave core operating lifetimes too short to be of interest, and enrichments of greater than 3.25 at. % U^{235} led to initial reactivities considered excessive from the standpoint of control problems. Due to the method by which the curves were computed, the values of reactivity predicted in the earlier portion of operating history are less than would be expected from two-group theory by about 1%. This difference becomes smaller as operating lifetime proceeds.

The initial conversion ratio (Figure 10) is defined as the number of plutonium atoms created for each U^{235} atom destroyed at the beginning of core life. These values were computed from the CANDLE four-group structure with the presence of control rods simulated by a homogenous poison. The appropriate four-group cross sections were used.

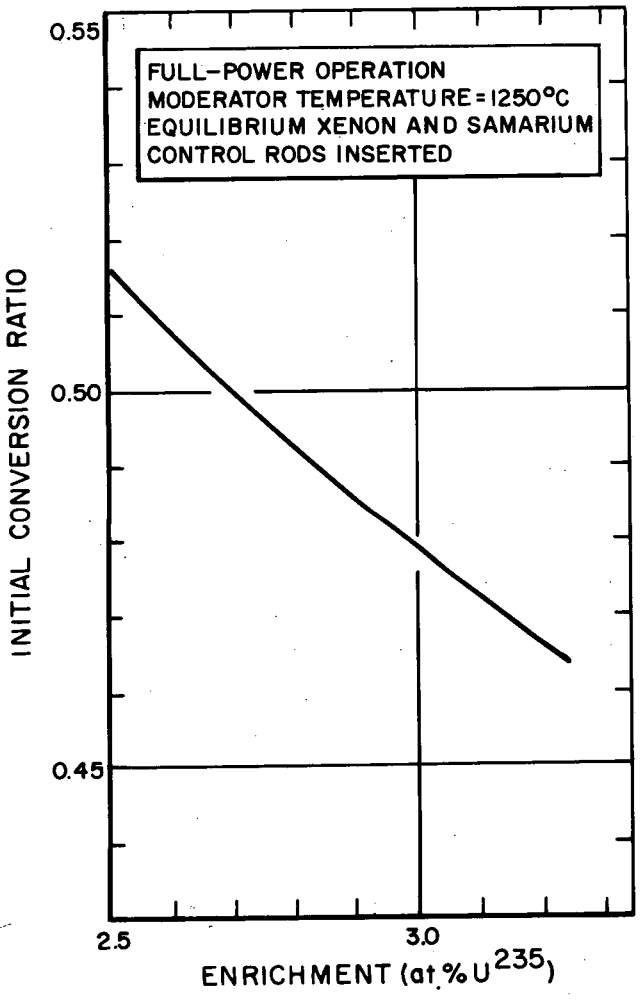

Figure 10. Variation of Initial Conversion Ratio with Enrichment in 255 Mwe ASGR

B. POWER DISTRIBUTION AND FUEL EXPOSURE

The remainder of the results are presented in eight sets of graphs for the four enrichments considered. The first set (Figures 11-A, 11-B, 11-C, and 11-D) shows the variation across the core of the ratio of the local radial power-generation rate to the average radial power-generation rate. The variation with burnup of this distribution is shown. The self-flattening effect produced as burnup proceeds is a result of the faster burnup of fissionable isotopes in the central portions of the core. This self-flattening is also the result of the particular control rod arrangement used. If the control rods were not uniformly distributed around the core, or were withdrawn in a nonuniform manner (e.g., outermost or intermost rods first) this flattening effect might be either accentuated or reduced.

The next graph (Figure 12) shows the ratios of radial peak fuel exposure to average radial fuel exposure as a function of average core exposure. This figure assumes angular symmetry and independence of local perturbations produced by control rod motion; it is based on an average value for the axial direction. In

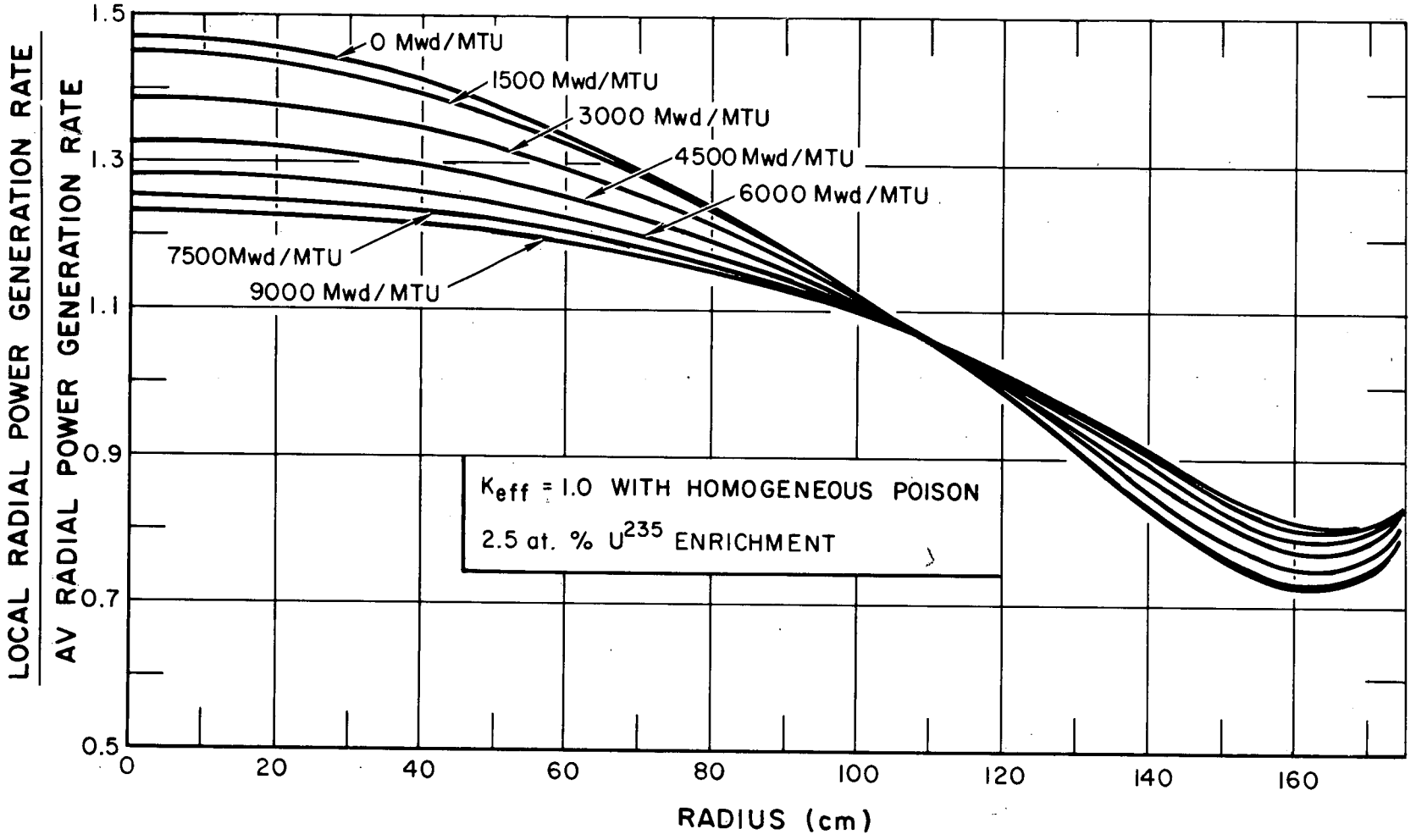

Figure 11A. Variation of Ratio of Local Radial Power Generation Rate to Average Radial Power Generation Rate with Burnup, 2.5 at. % U^{235} Enrichment

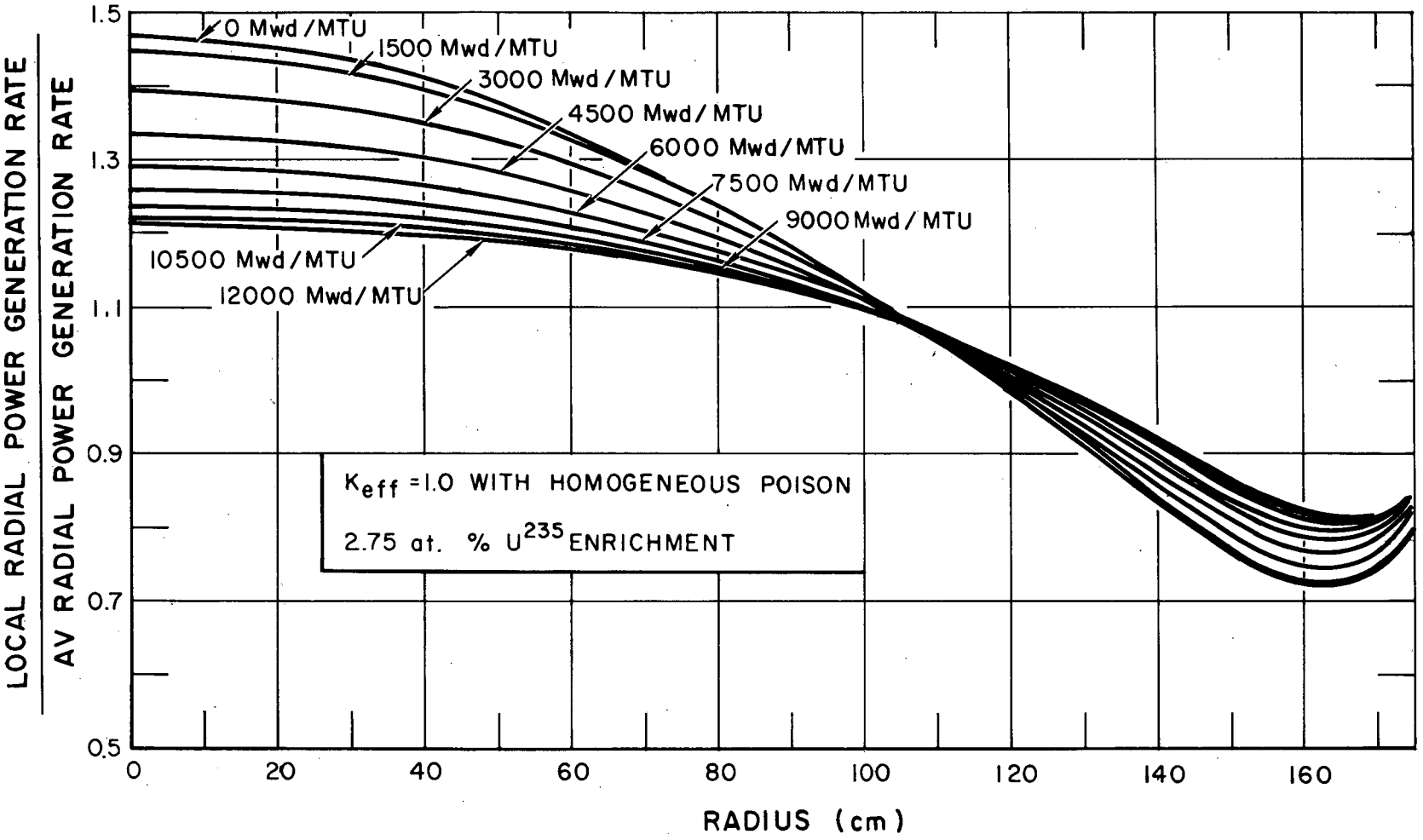

Figure 11B. Variation of Ratio of Local Radial Power Generation Rate to Average Radial Power Generation Rate with Burnup, 2.75 at. % U^{235} Enrichment

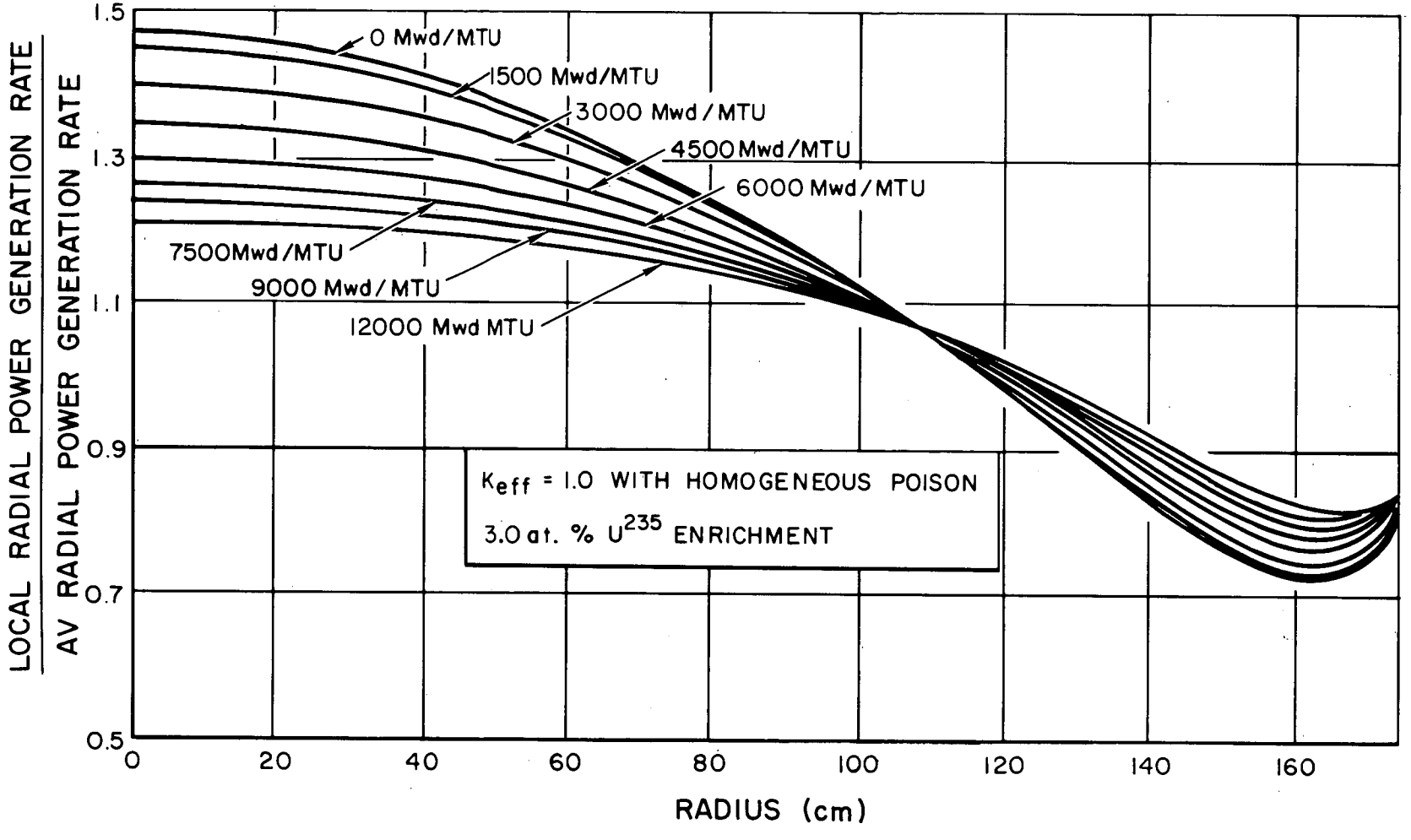

Figure 11C. Variation of Ratio of Local Radial Power Generation Rate to Average Radial Power Generation Rate with Burnup, 3.0 at. % U^{235} Enrichment

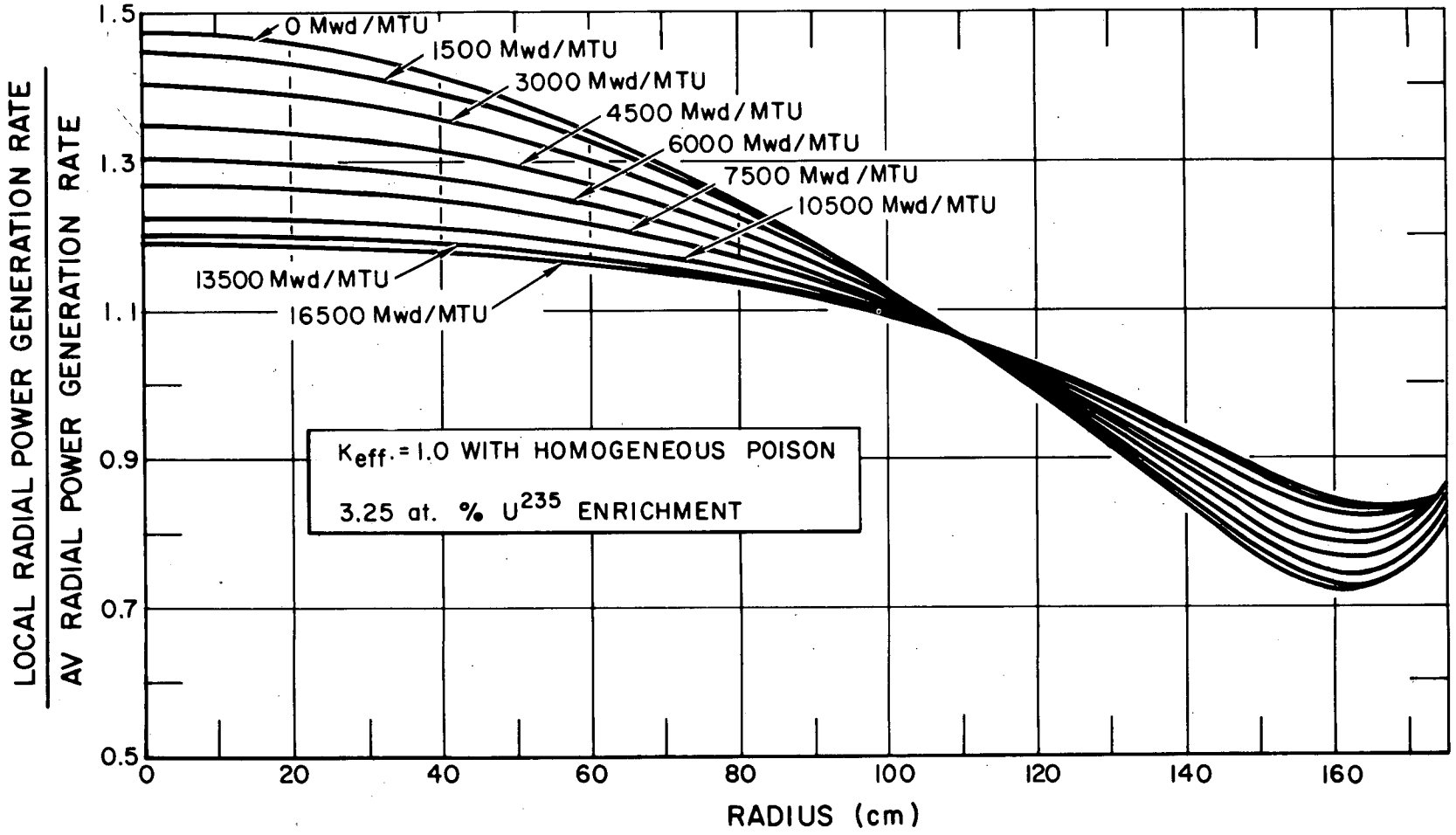

Figure 11D. Variation of Ratio of Local Radial Power Generation Rate to Average Radial Power Generation Rate with Burnup, 3.25 at. % U^{235} Enrichment

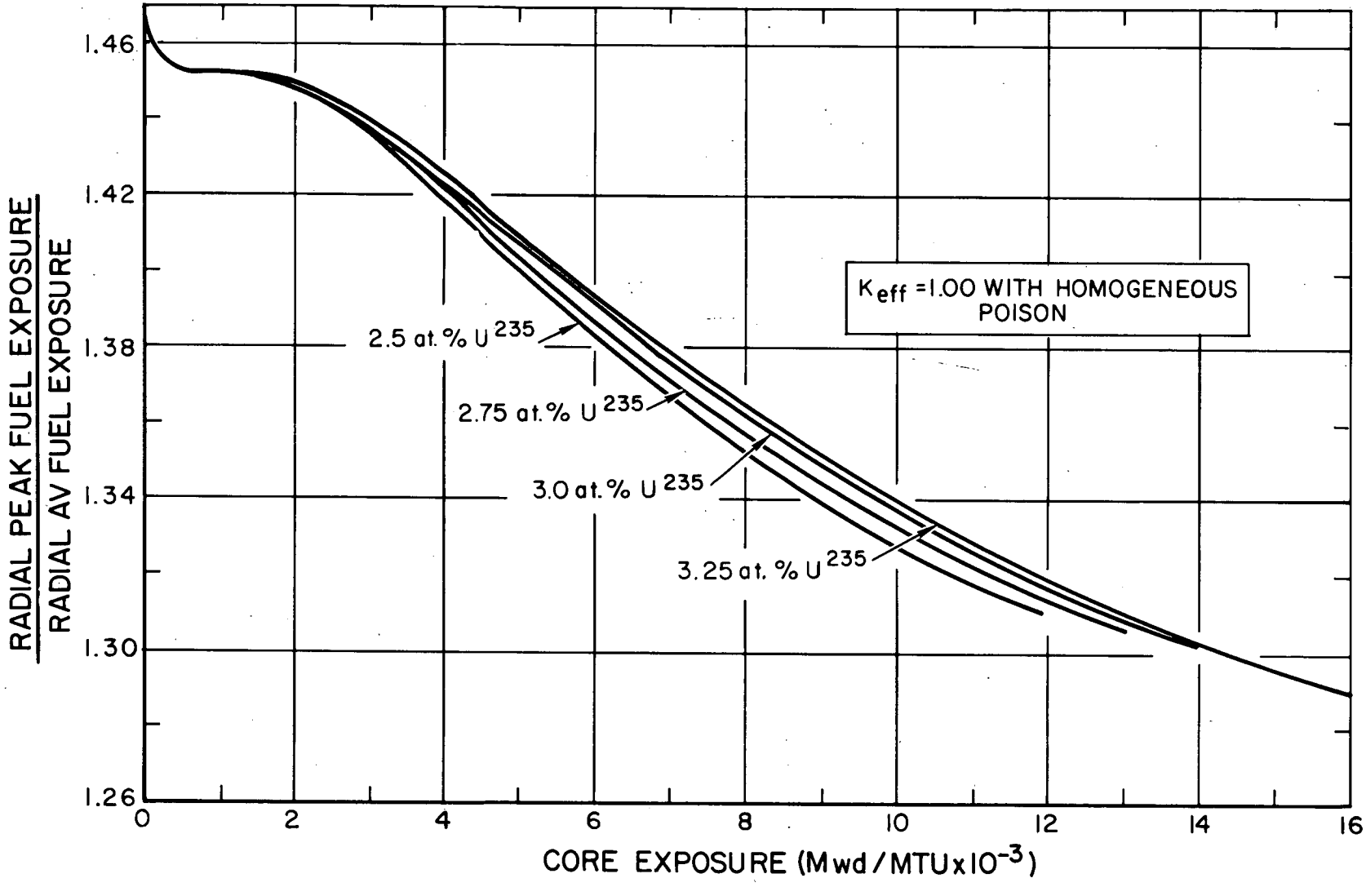

Figure 12. Variation of Ratio of Radial Peak Fuel Exposure to Radial Average Fuel Exposure with Burnup

order to arrive at a peak fuel exposure for any average core-exposure, it is necessary to know also the power distribution in the axial direction and within a fuel cluster. The power distribution and the rate of fuel element exposure in the axial direction depend on the control-rod program. Since this study was one dimensional, there is no information on this effect. The simplest assumption that can be made about the control-rod program is that the rods are not banked, and that individual rods are either fully inserted or fully withdrawn. In this case they would not be expected to disturb the axial flux shape, and there would be a self-flattening in the axial direction, as in the radial. The initial value of the peak-to-average power generation rate in the axial direction is 1.340. This value may be used with the reservation that it will lead to an over estimate of the peak fuel-exposure.

The complex question of peak-to-average power generation within a 19-rod fuel cluster has been examined elsewhere.[16] Experimental measurements (with 2.78 wt % enriched uranium metal fuel) have been performed on a cluster of 19 rods, each 3/4 in. in diameter.[17] These measurements showed that, at room temperature, the peak-to-average thermal-flux distribution was 1.326. For the cluster considered here (with rods of smaller diameter, fuel of lower density and higher neutron temperature) this value would be expected to be smaller. A calculational model was adopted which predicted, within 2%, the peak-to-average thermal-flux distribution in the experimental cluster. Using this model, the peak-to-average thermal-flux distribution in the lattice for the 255 Mwe ASGR was calculated. Approximately 27% of the total power is generated by fissions due to fast neutrons (Table IV). It was assumed that the fast neutron flux was spatially flat across a fuel cluster, and the peak-to-average power generation rate in a fuel cluster was calculated. The values of peak-to-average power-generation rate ranged approximately linearly from 1.068 for 2.5 at. % U^{235} enriched fuel to 1.078 for 3.25 at. % U^{235} enriched fuel.

As burnup proceeds, the outer rods in the cluster will become exposed more rapidly than the inner rods. Since the thermal-absorption cross-section of the fuel increases with exposure, the cluster will become "blacker" to thermal neutrons, and the peak-to-average thermal flux across the cluster will increase. At the same time, due to the difference in exposure, the thermal macroscopic fission cross section in the outer rods will increase more rapidly than in the

inner rods, and the peak-to-average power distribution will increase still further. The reasons for these changes in thermal cross section with exposure will be discussed in the following section in connection with Figure 17.

There will also be preferential resonance absorption of neutrons by U^{238} to form plutonium in the outer rods. These factors will all tend to accentuate the difference between the inner and outer rods and give a greater peak-to-average fuel exposure in a cluster than that predicted by the initial value. The fact that the initial value will underestimate the peak fuel exposure in a cluster will partially compensate for the over estimate of peak exposure in the axial direction, given by the use of the initial power distribution.

Figure 13 shows the variation in the ratio of the maximum radial power-generation rate to the average radial power-generation rate with burnup.

Variation with average core exposure of the average exposure of the fuel within any radial fraction of the core volume is indicated in Figures 14-A, 14-B, 14-C, and 14-D. From these curves and from interpolations that can be made between the curves, one can obtain the average radial exposure of the fuel removed from within any region of the core. Since, for a first reloading, the fuel at the center of the core is always most exposed if the reloading is in a region that includes the center of the core, both the average exposure of the removed fuel and the ratio of radial peak-to-average exposure in the removed fuel are known.

C. ISOTOPIC COMPOSITION

The variation in fuel composition with burnup is shown in Figures 15-A, 15-B, 15-C, and 15-D. The relationship between the amount of U^{235} consumed in fission and that converted to U^{236} is not quite constant. This ratio is dependent on the spectrum, which is in turn somewhat dependent on the enrichment and burnup. An average value for this reactor that will be correct to within 1% is 0.275 atoms of U^{236} formed for each U^{235} atom consumed in fission. The shaded area in Figure 15 shows the amount of U^{235} fissioned plus the amount of U^{238} converted to plutonium and fissioned as Pu^{239} or Pu^{241}. The amount of plutonium (all isotopes) remaining in the fuel is also shown. As enrichment increases, the amount of U^{235} that has been consumed in fission at any given

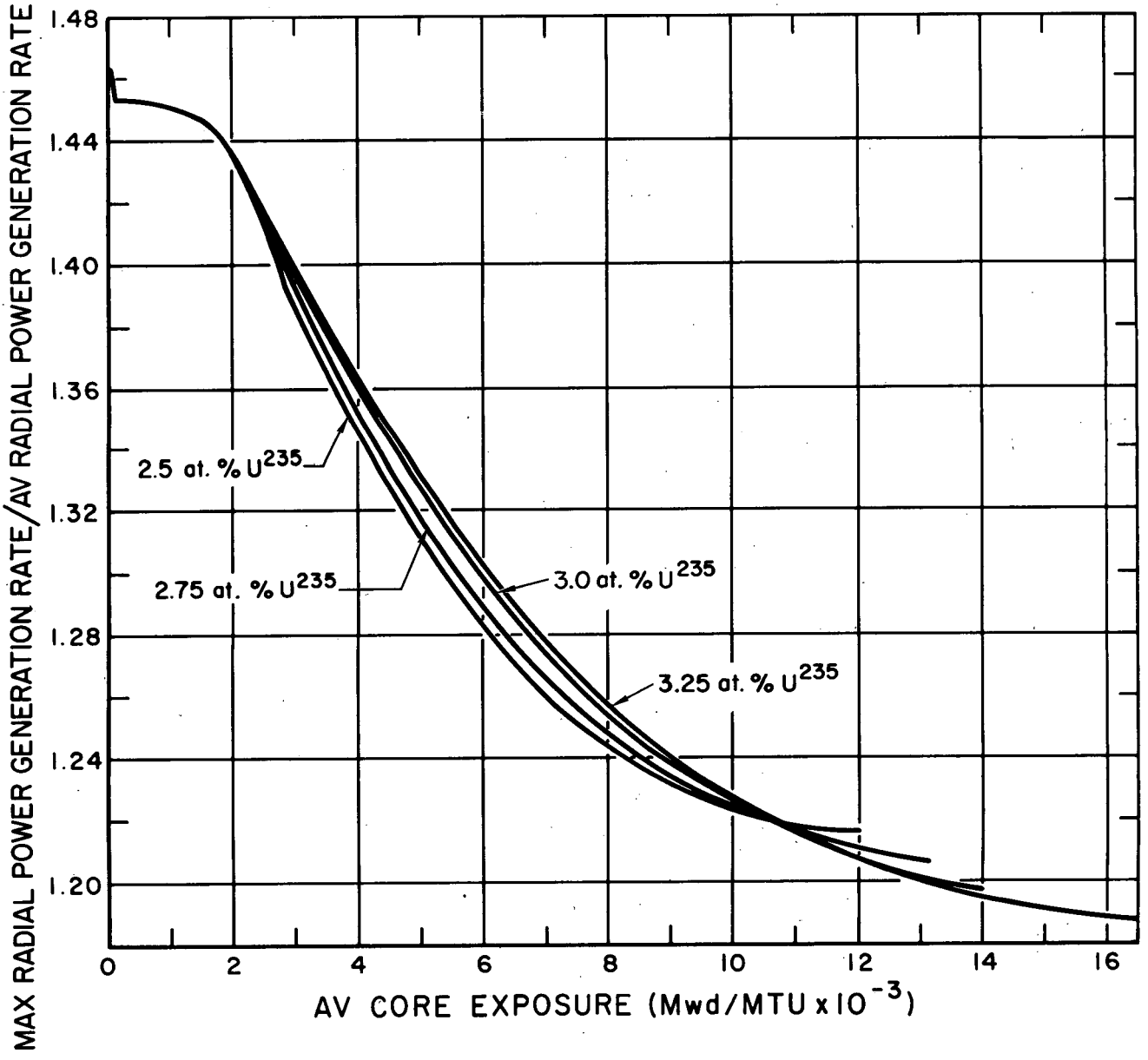

Figure 13. Variation of Ratio of Maximum Radial Power Generation Rate to Average Radial Power Generation Rate with Burnup

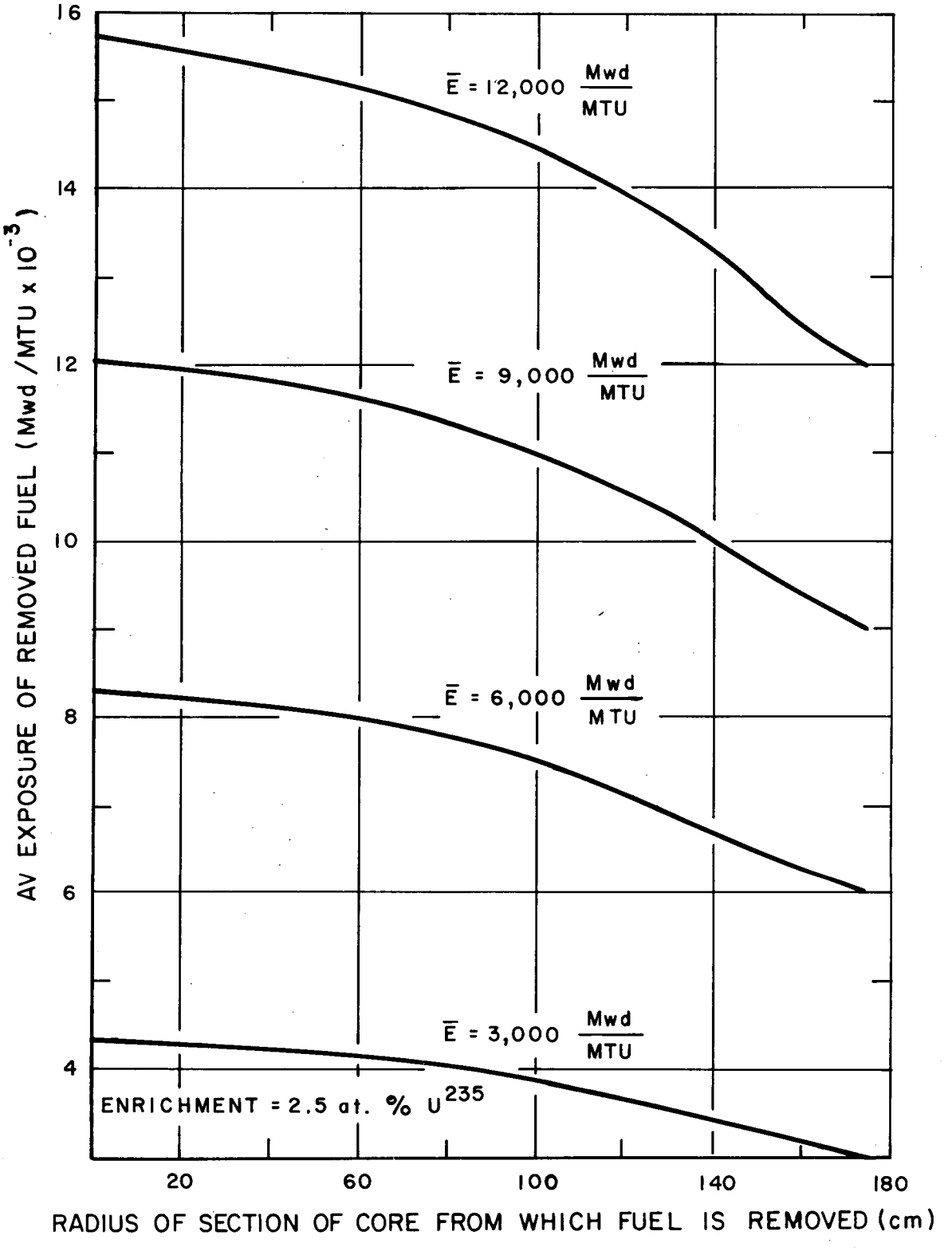

Figure 14A. Average Exposure of Fuel Removed from Core, 2.5 at. % U^{235} Enrichment

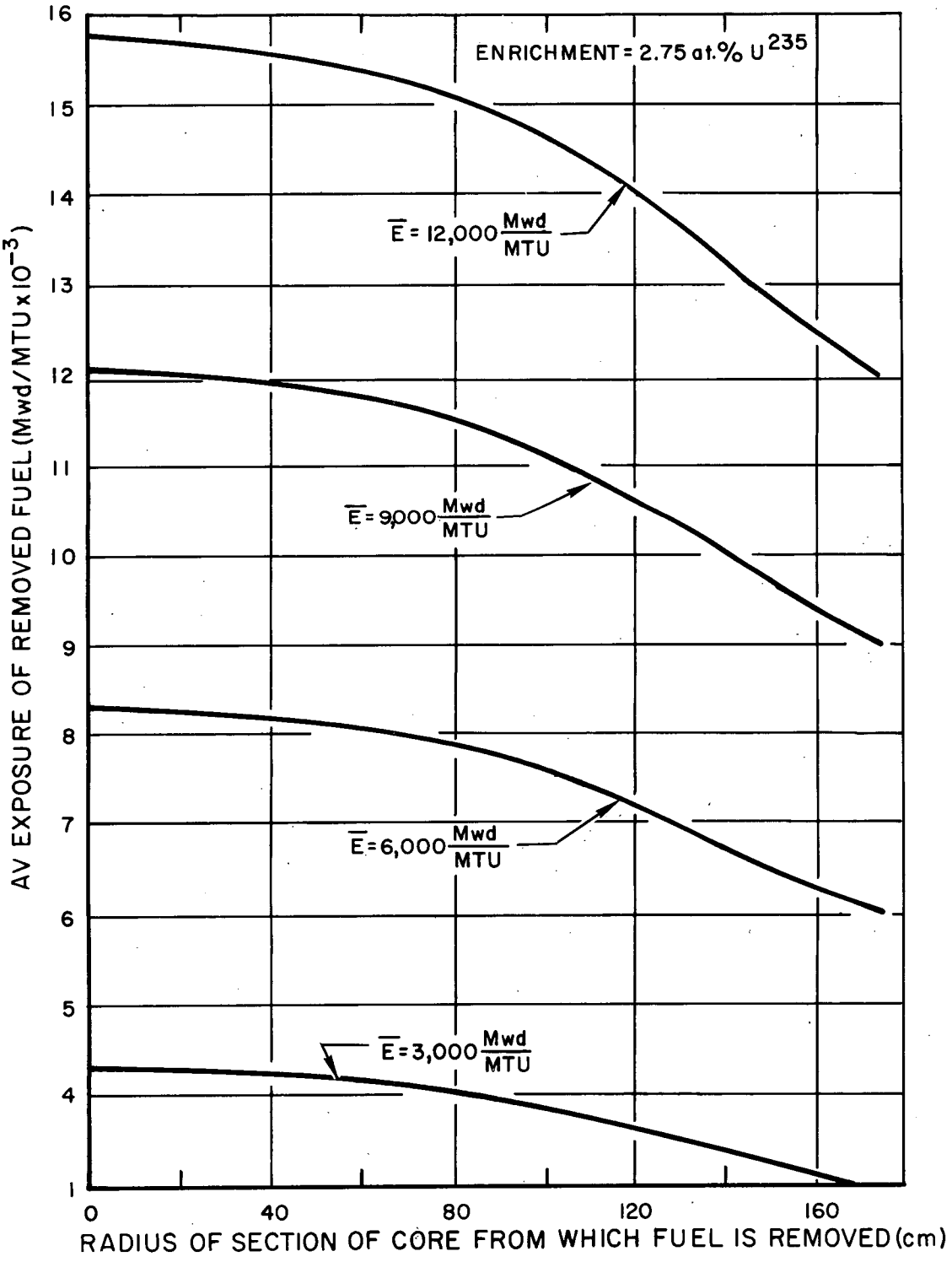

Figure 14B. Average Exposure of Fuel Removed from Core, 2.75 at. % U^{235} Enrichment

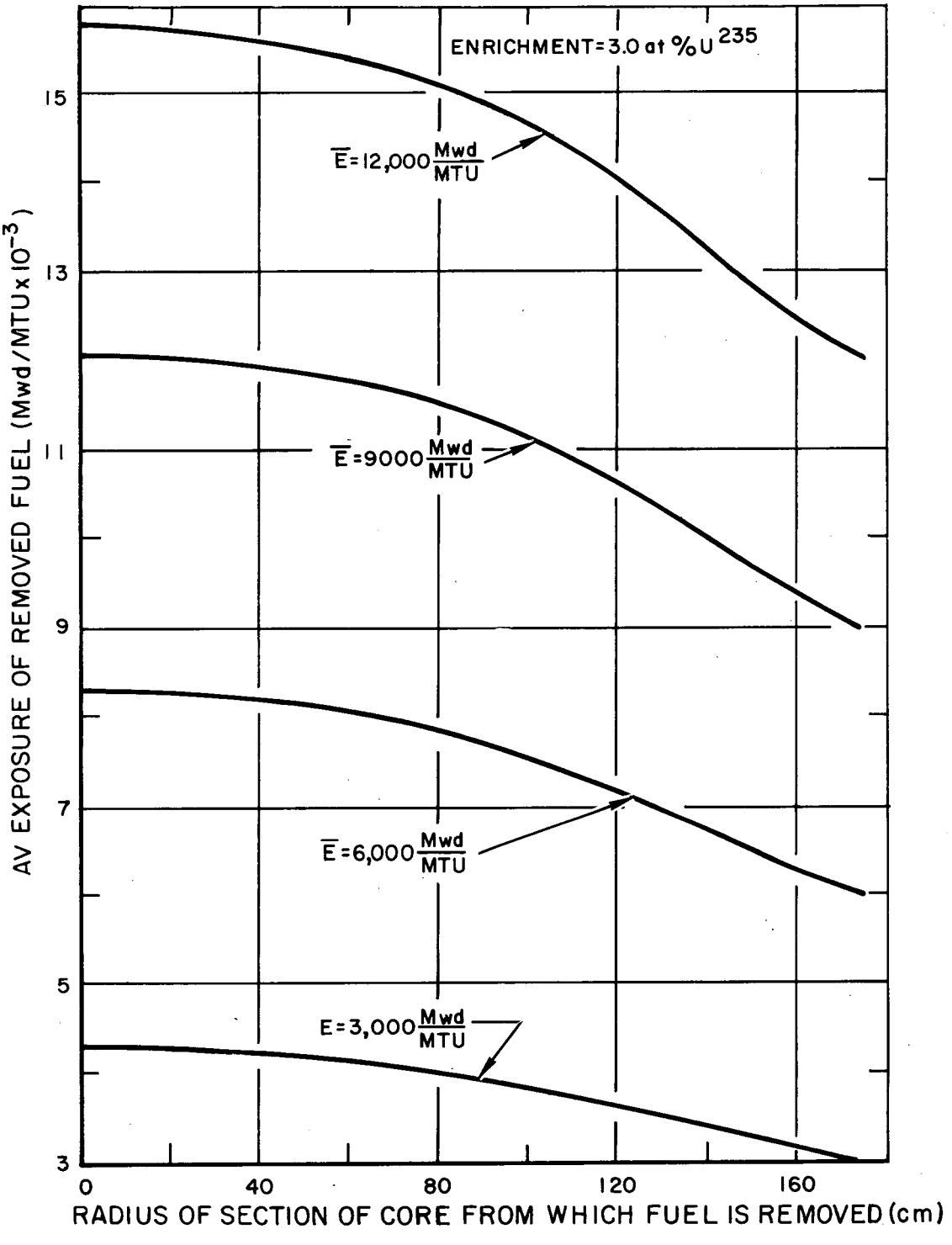

Figure 14C. Average Exposure of Fuel Removed from Core, 3.0 at. % U^{235} Enrichment

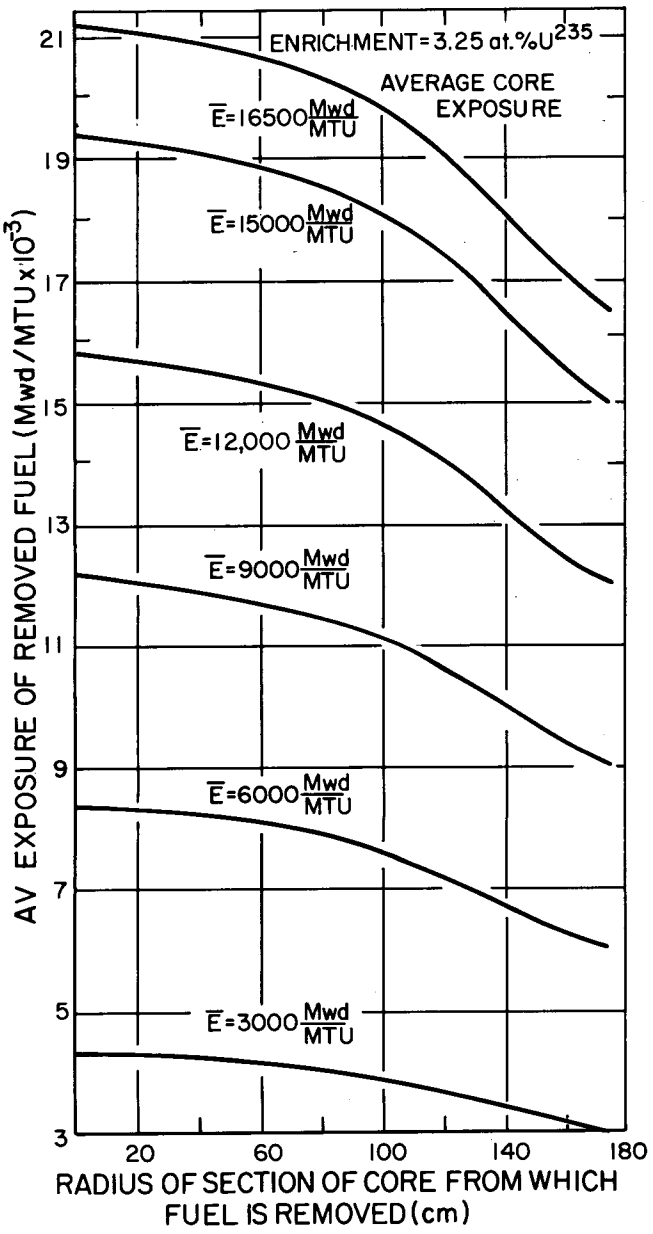

Figure 14D. Average Exposure of Fuel Removed from Core, 3.25 at. % U^{235} Enrichment

burnup also increases. In addition, the conversion ratio is smaller, and a smaller amount of plutonium is formed in cores with higher enrichment. Approximately the same amount of plutonium remains in the core at any given burnup, regardless of enrichment. This means that a smaller amount of plutonium has been fissioned, and a larger percentage of the power is generated from fissions in U^{235}.

The composition of the plutonium remaining in the core as a function of burnup is indicated in Figures 16-A, 16-B, 16-C, and 16-D. The ratio of the concentrations of the isotopes depends on the relative cross sections. At the neutron temperatures used, the thermal capture-to-fission ratio is high for Pu^{239}. This is the reason for the large concentration of Pu^{240} and Pu^{241} relative to Pu^{239}. The predicted equilibrium concentration of the three principal plutonium isotopes is approximately 26% Pu^{239}, 21% Pu^{240}, and 53% Pu^{241}.

The effects of changes in fuel isotopic composition on macroscopic cross-section are shown in Figures 17-A, 17-B, 17-C, and 17-D. These include the effects of fission products. The principal effects are due to changes in the relative fissionable and fertile isotope concentrations. Though less than one Pu^{239} atom is produced for each U^{235} atom destroyed, the cross sections of Pu^{239} are much higher than those of U^{235}, and the macroscopic fuel cross

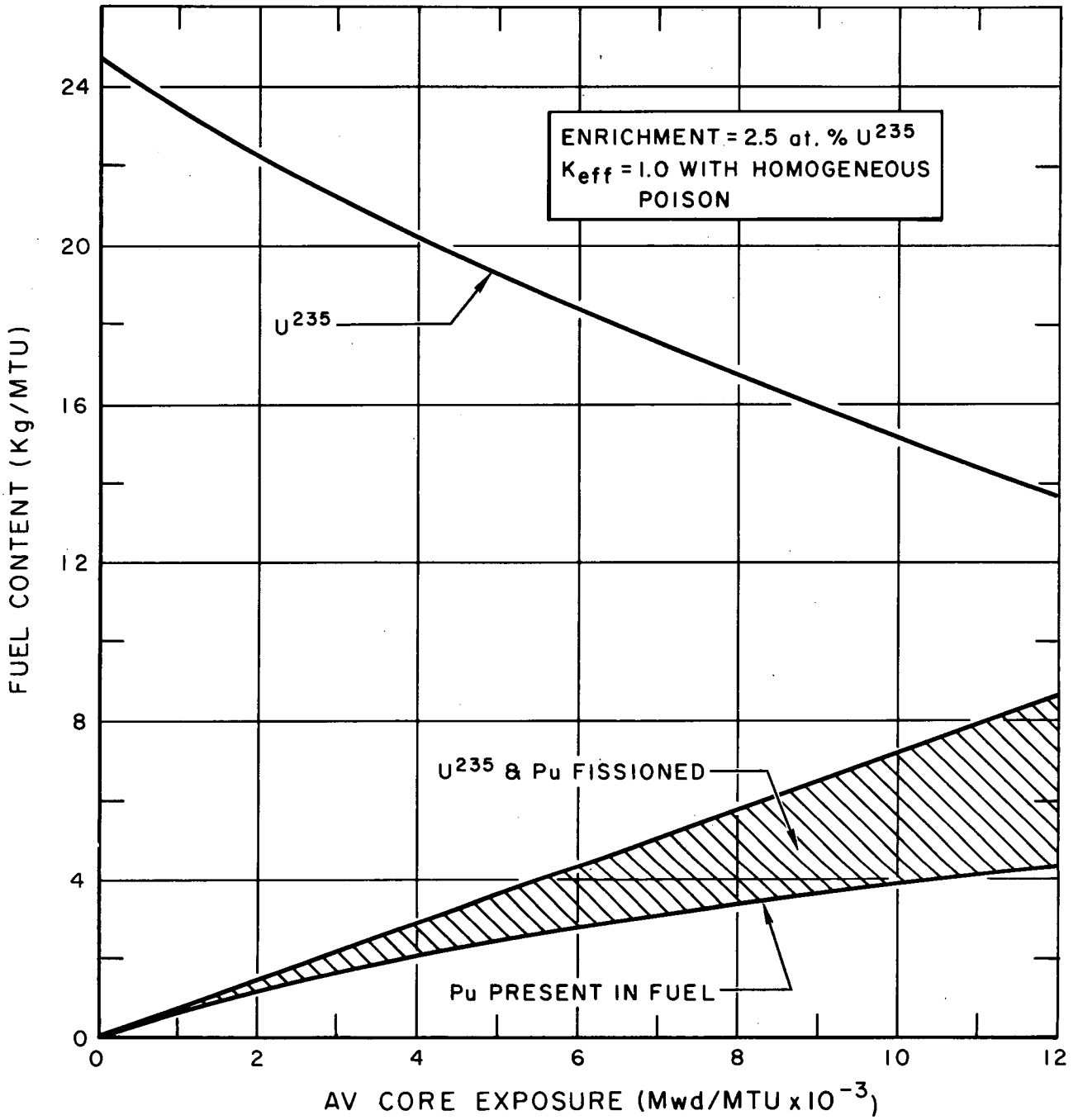

Figure 15A. Variation in Fuel Composition with Burnup, 2.5 at. % U^{235} Enrichment

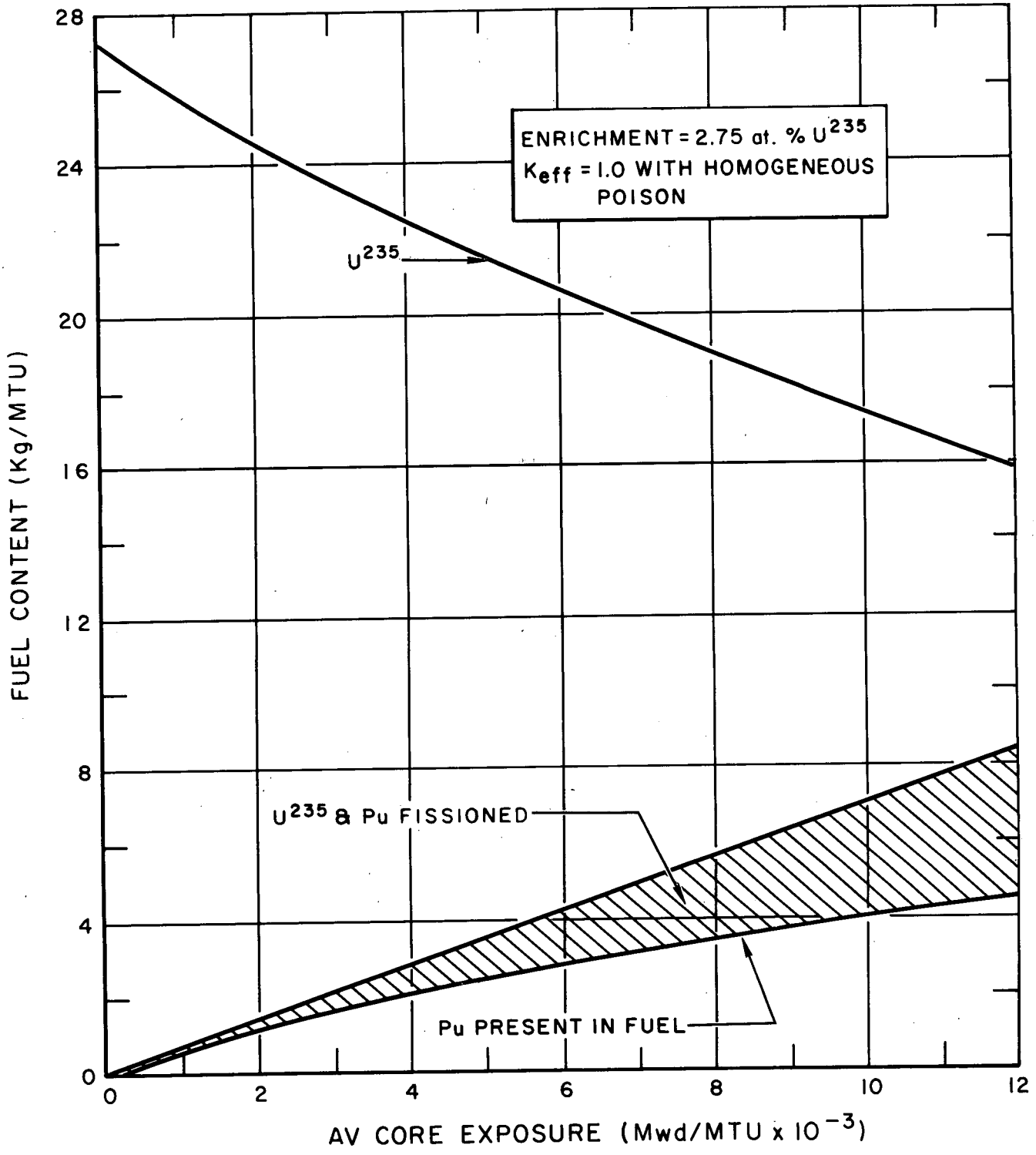

Figure 15B. Variation in Fuel Composition with Burnup, 2.75 at. % U^{235} Enrichment

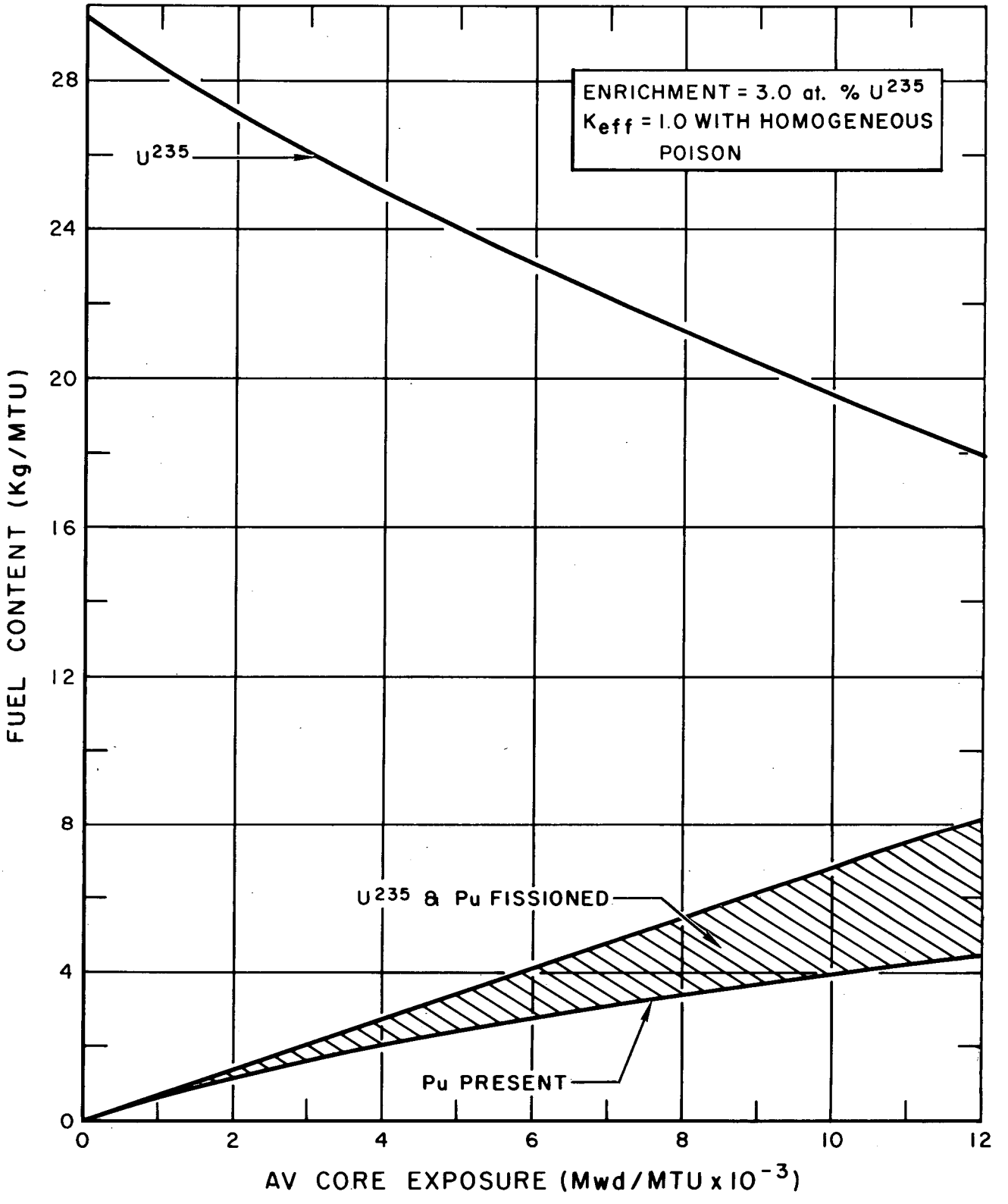

Figure 15C. Variation in Fuel Composition with Burnup, 3.0 at. % U^{235} Enrichment

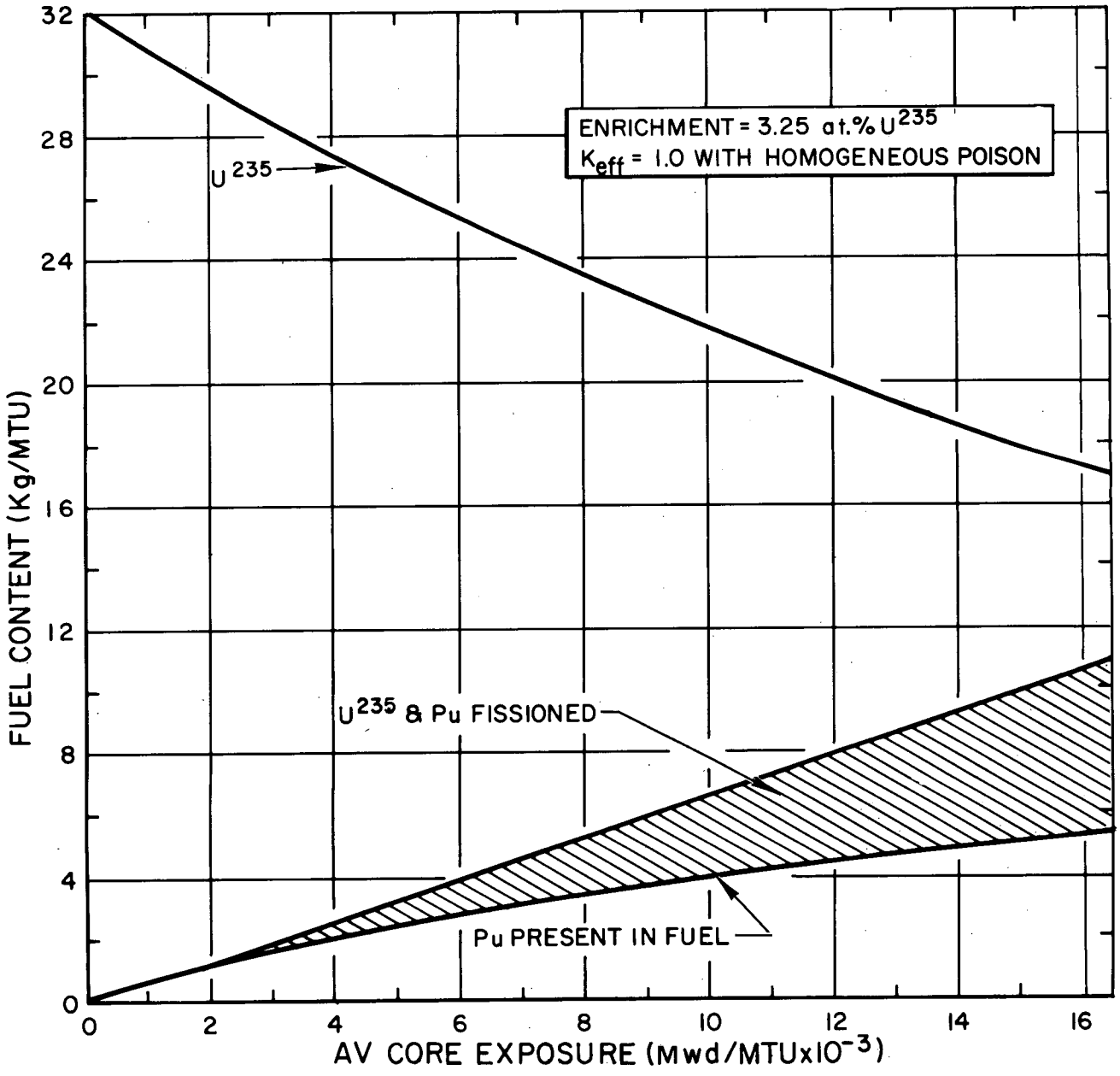

Figure 15D. Variation in Fuel Composition with Burnup, 3.25 at. % U^{235} Enrichment

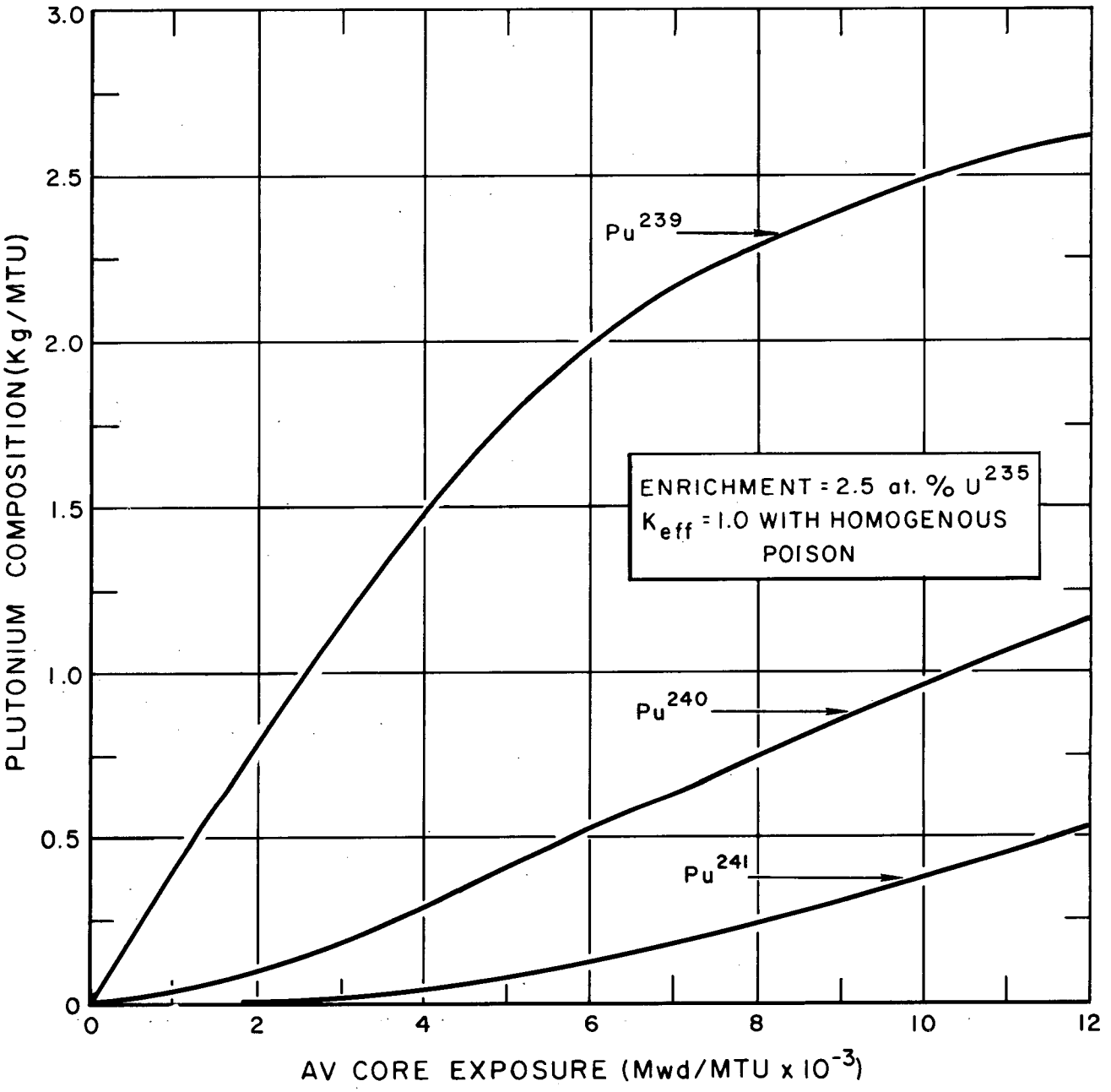

Figure 16A. Composition of Plutonium Remaining in Core as a Function of Burnup, 2.5 at. % U^{235} Enrichment

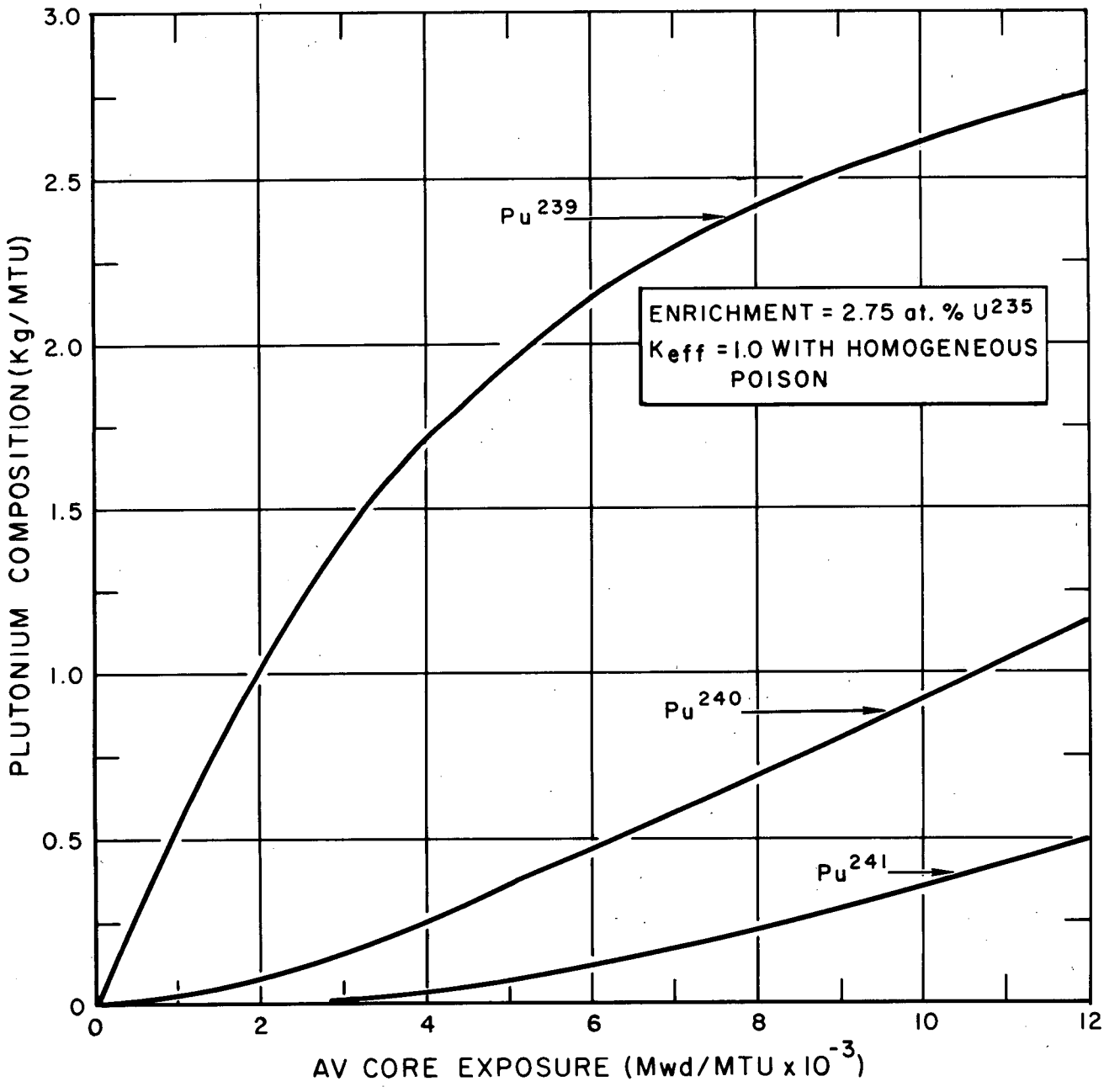

Figure 16B. Composition of Plutonium Remaining in Core as a Function of Burnup, 2.75 at. % U^{235} Enrichment

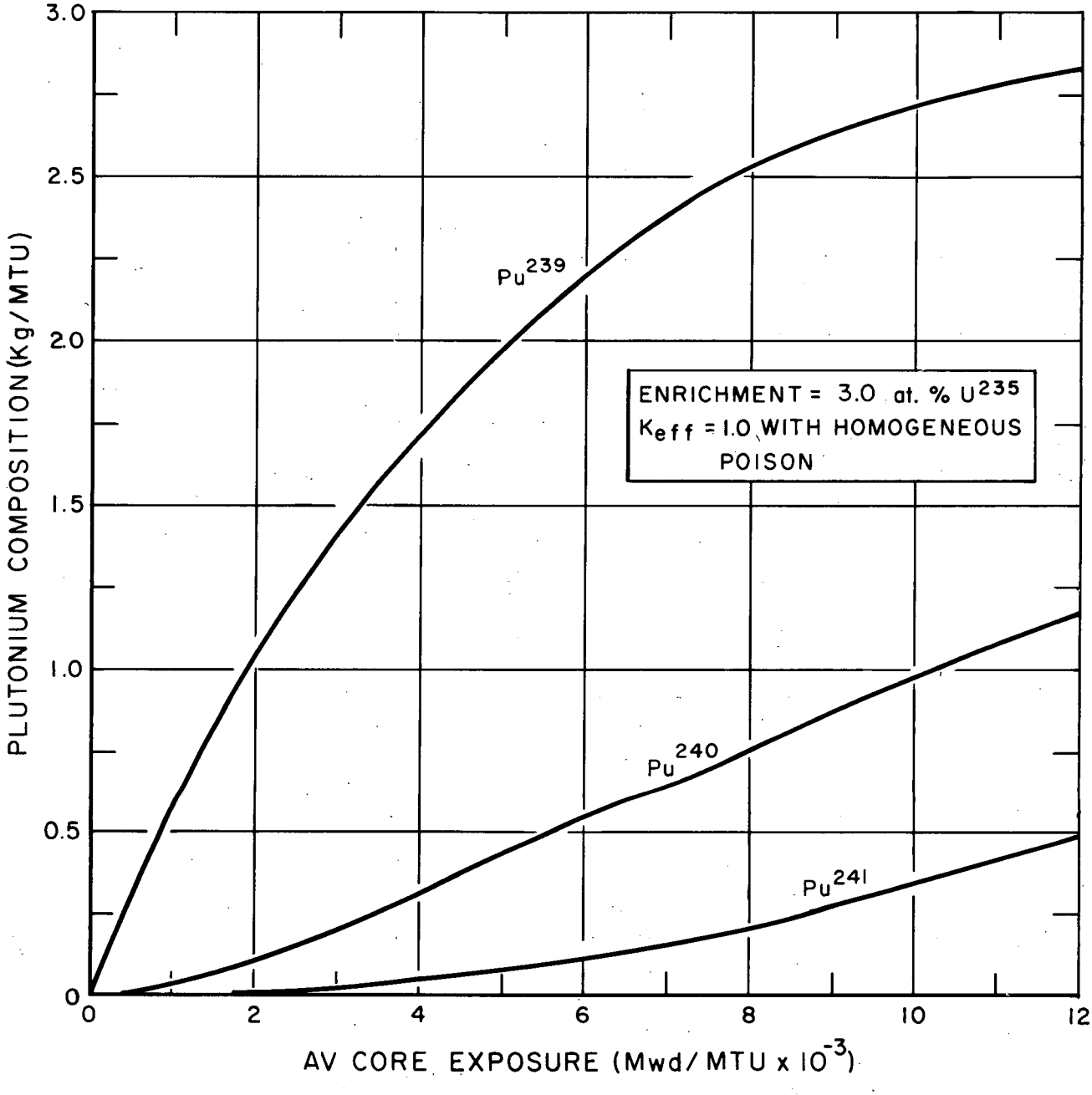

Figure 16C. Composition of Plutonium Remaining in Core as a Function of Burnup, 3.0 at. % U^{235} Enrichment

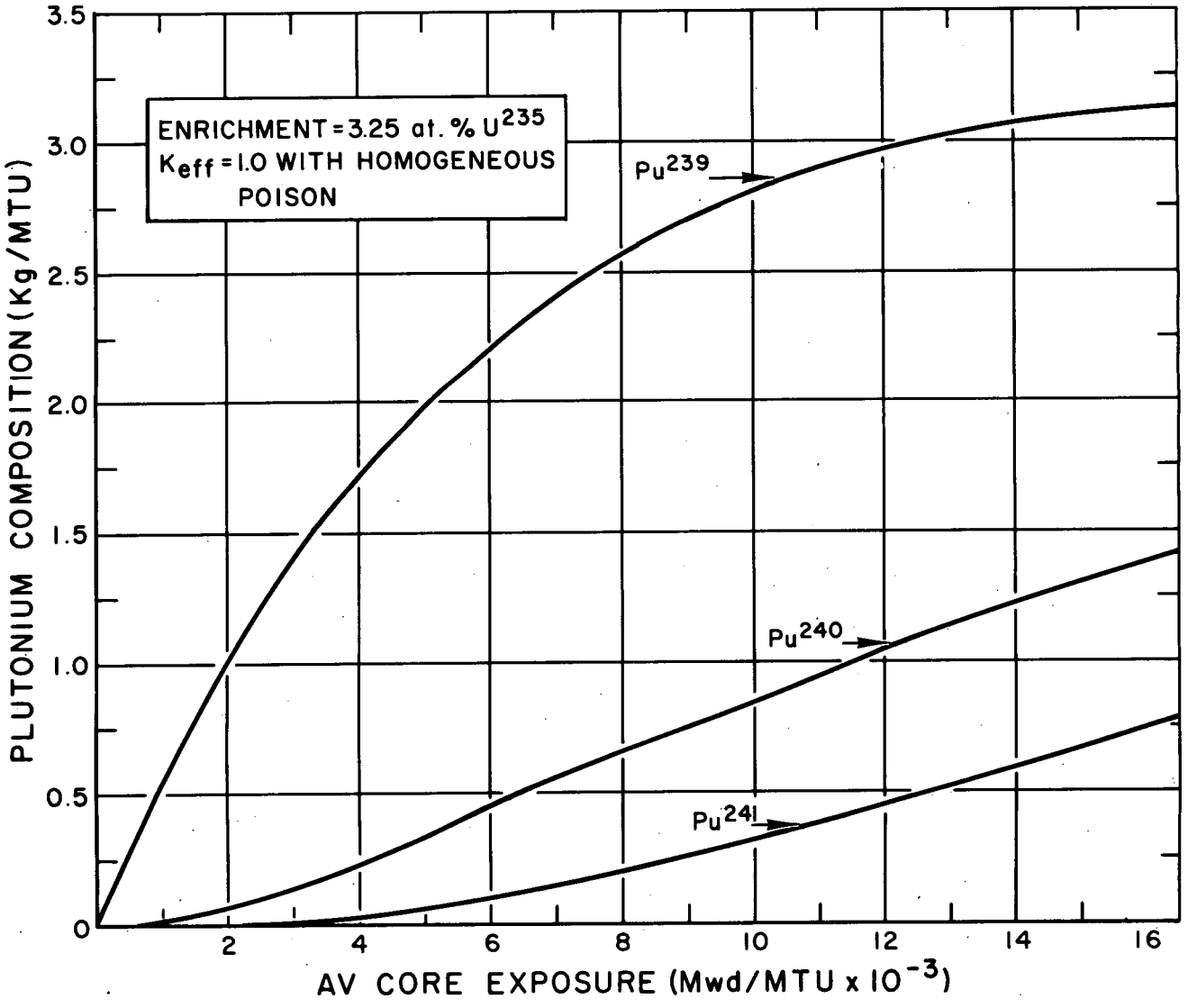

Figure 16D. Composition of Plutonium Remaining in Core as a Function of Burnup, 3.25 at. % U^{235} Enrichment

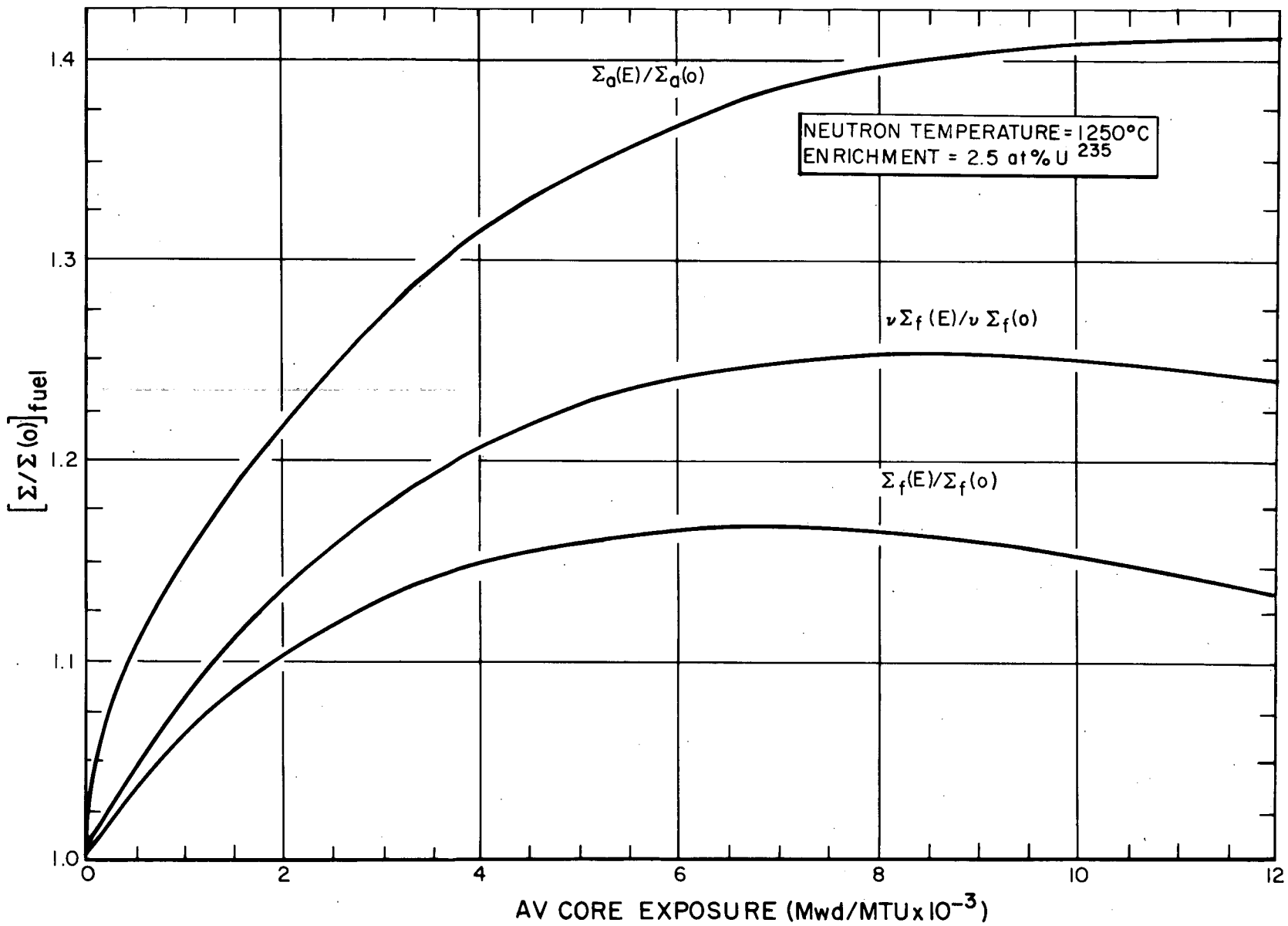

Figure 17A. Variation of Fuel Macroscopic Thermal Cross-Sections with Burnup, 2.5 at. % U^{235} Enrichment

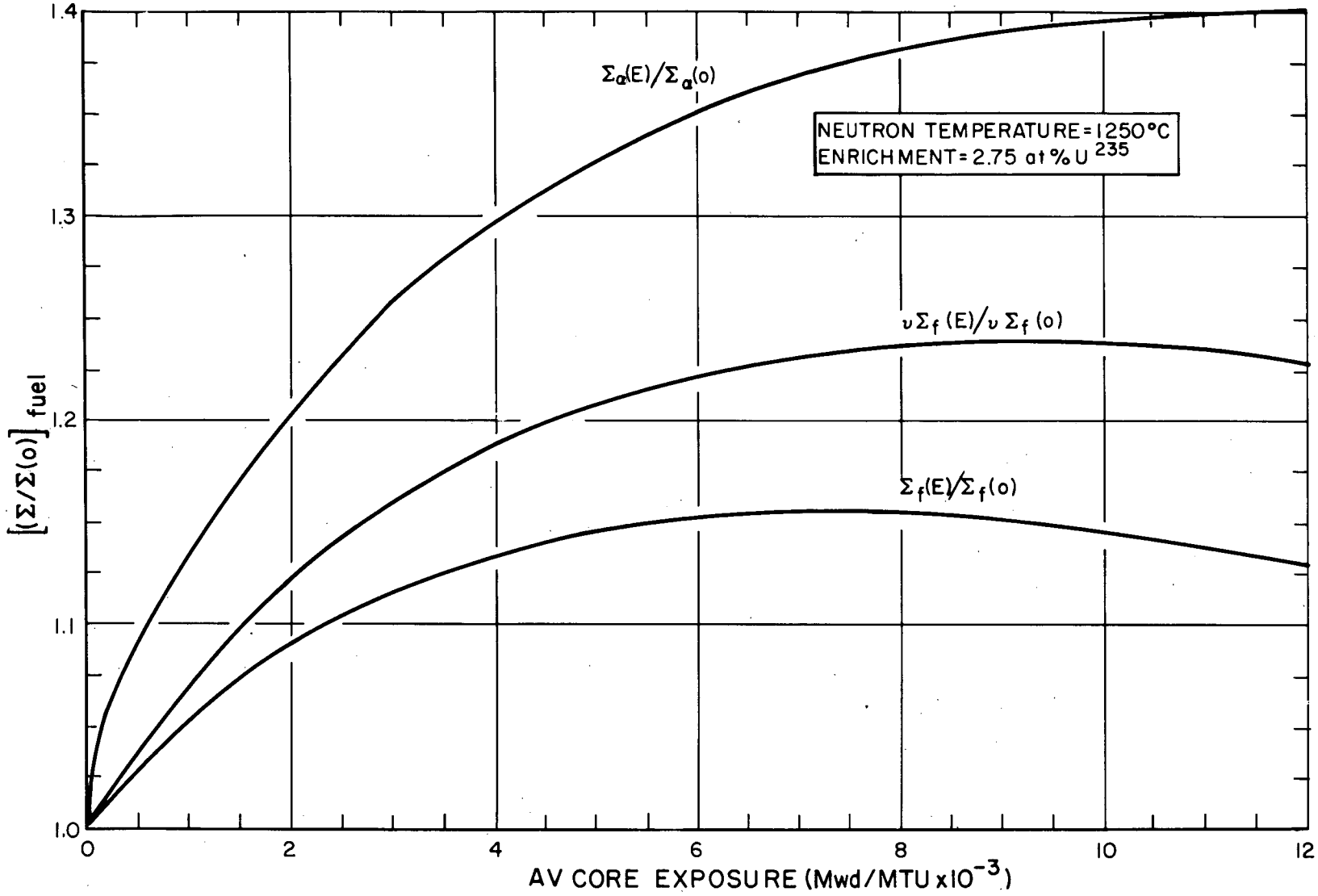

Figure 17B. Variation of Fuel Macroscopic Thermal Cross-Sections with Burnup, 2.75 at. % U^{235} Enrichment

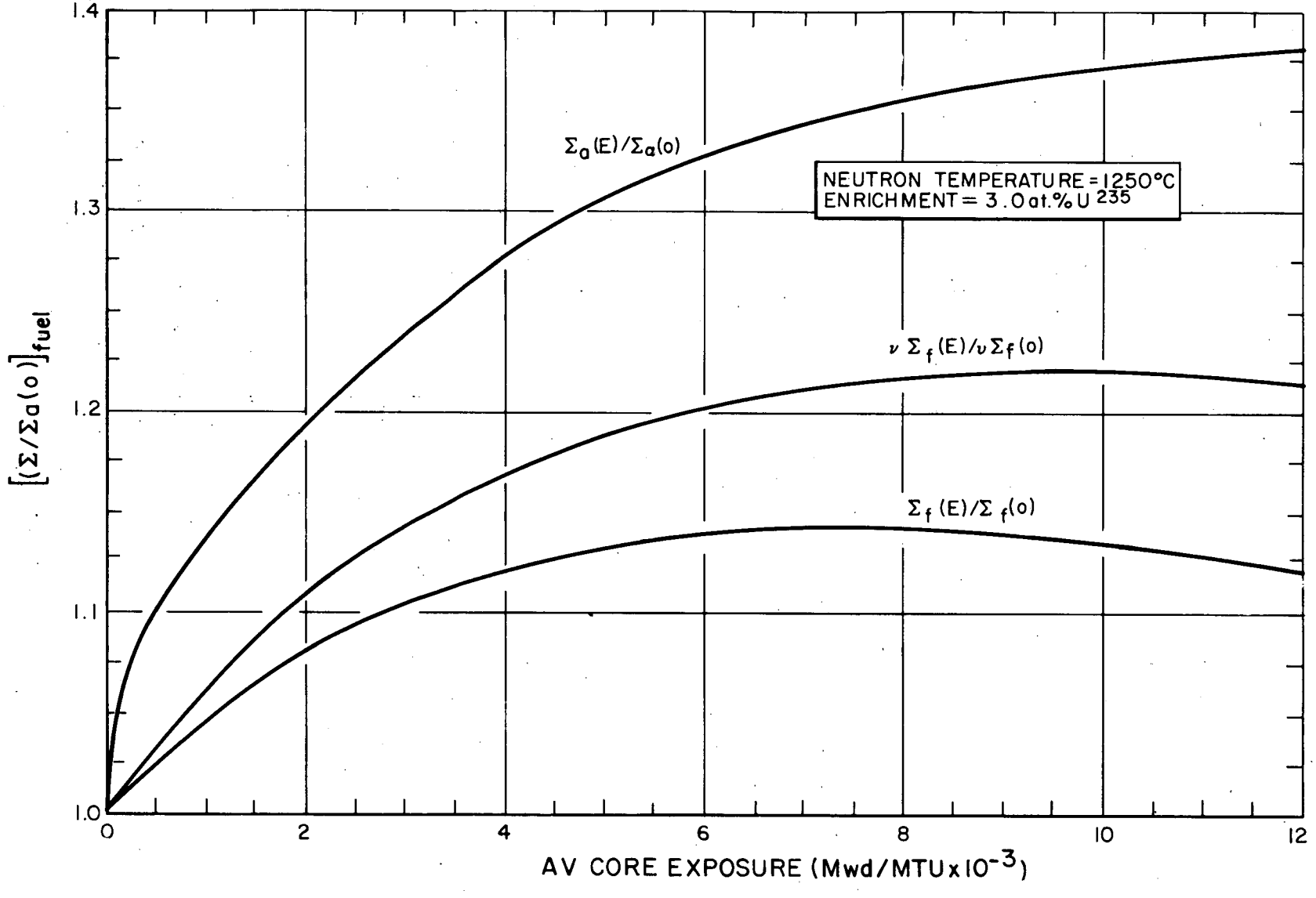

Figure 17C. Variation of Fuel Macroscopic Thermal Cross-Sections with Burnup, 3.0 at. % U^{235} Enrichment

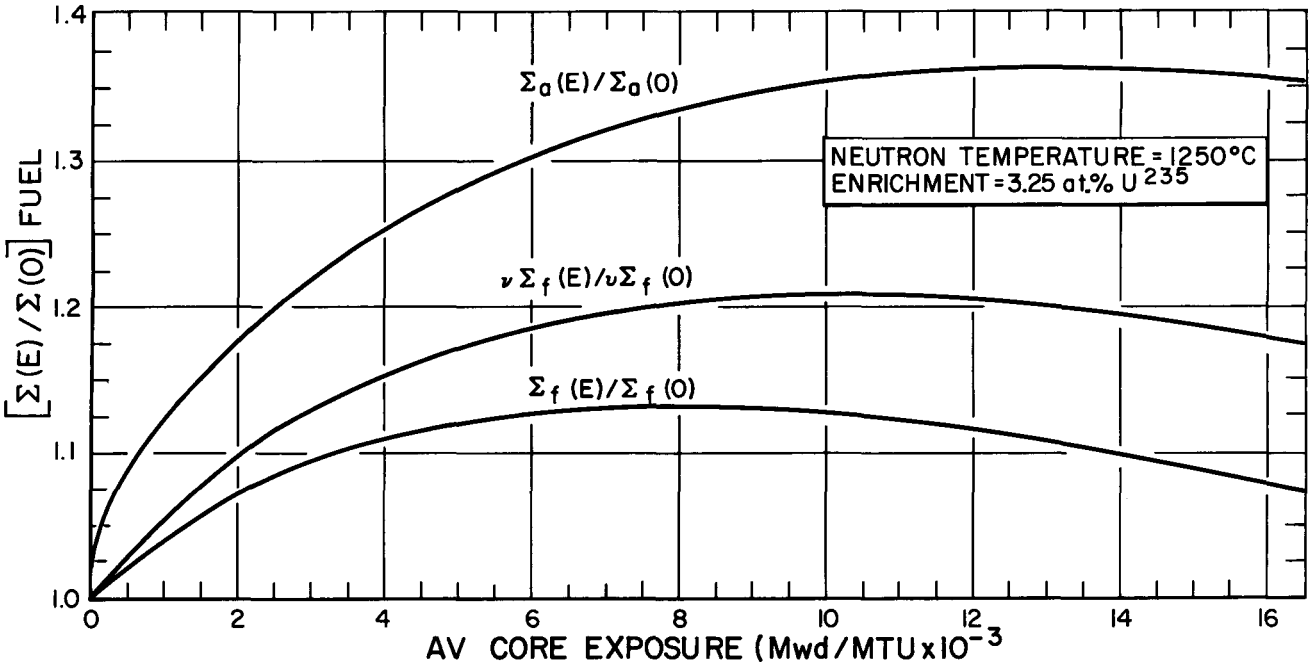

Figure 17D. Variation of Fuel Macroscopic Thermal Cross-Sections with Burnup, 3.25 at. % U^{235} Enrichment

sections show an increase with burnup. Eventually, at high burnups, the plutonium approaches an equilibrium concentration but the U^{235} depletion continues. The net result is an eventual decrease in cross sections.

Contributions of each of the fissionable isotopes to total power generation may be seen in Figures 18-A, 18-B, 18-C, and 18-D. The importance of the plutonium contribution to power generation, as well as the dependence of this contribution on enrichment, can be assessed from these figures.

The decrease of available reactivity due to the xenon buildup after a reduction in power is shown in Figure 19. The plot was based on a two-group formulation, and is for 2.75 at. % U^{235} enriched fuel. Production of Xe^{135} was taken to result from fast and thermal fissions, but removal through neutron absorption was due only to absorption of thermal neutrons. At full-power operation, the Δk_{eff} due to the presence of an equilibrium concentration of Xe^{135} is -0.0345. After a reduction in power level, the Xe^{135} concentration (and the loss in reactivity due to parasitic capture in Xe^{135}) increases for a time. This is because

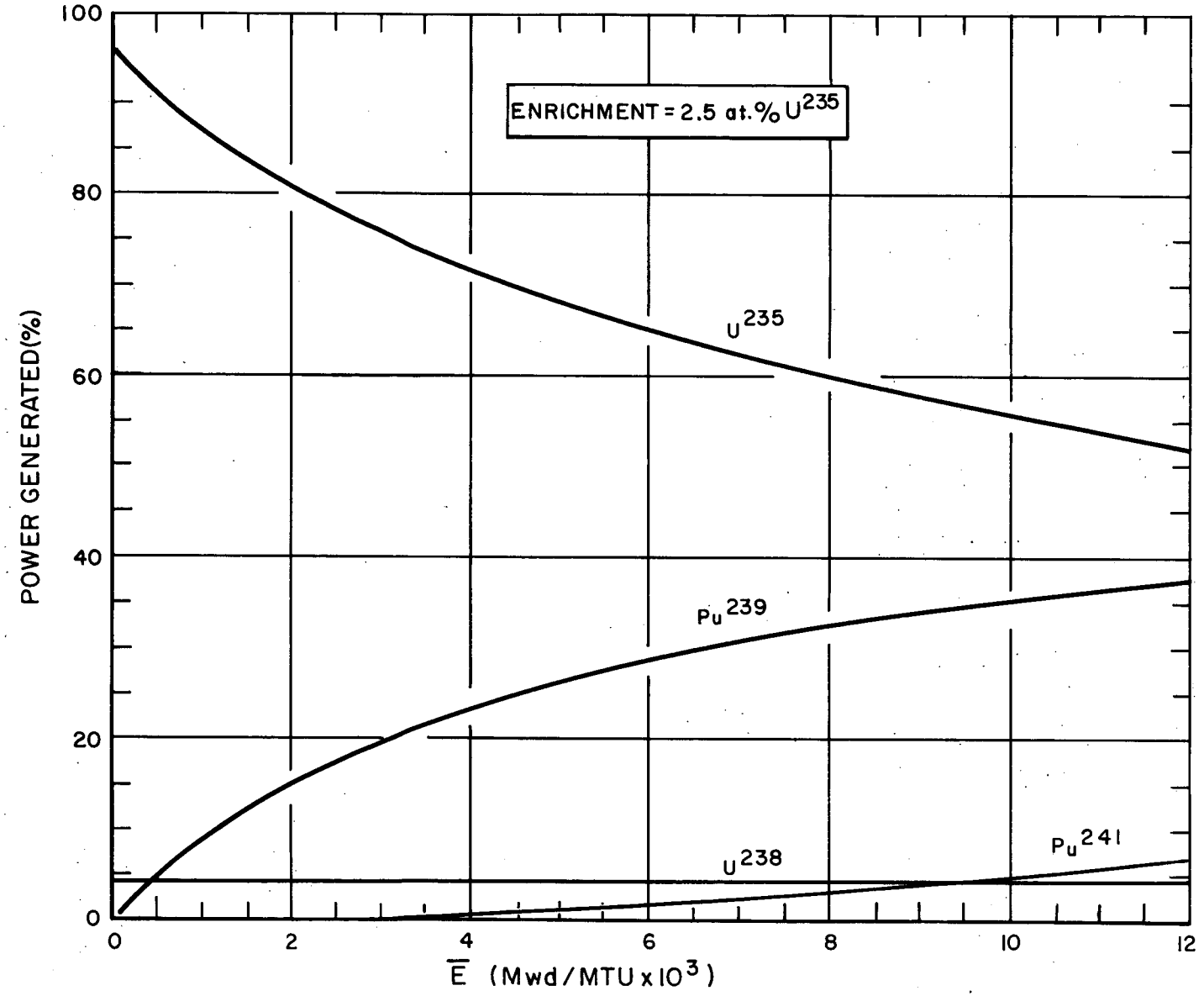

Figure 18A. Variation in Percentage of Total Power Generated by Each Fissionable Isotope as a Function of Burnup, 2.5 at. % U^{235} Enrichment

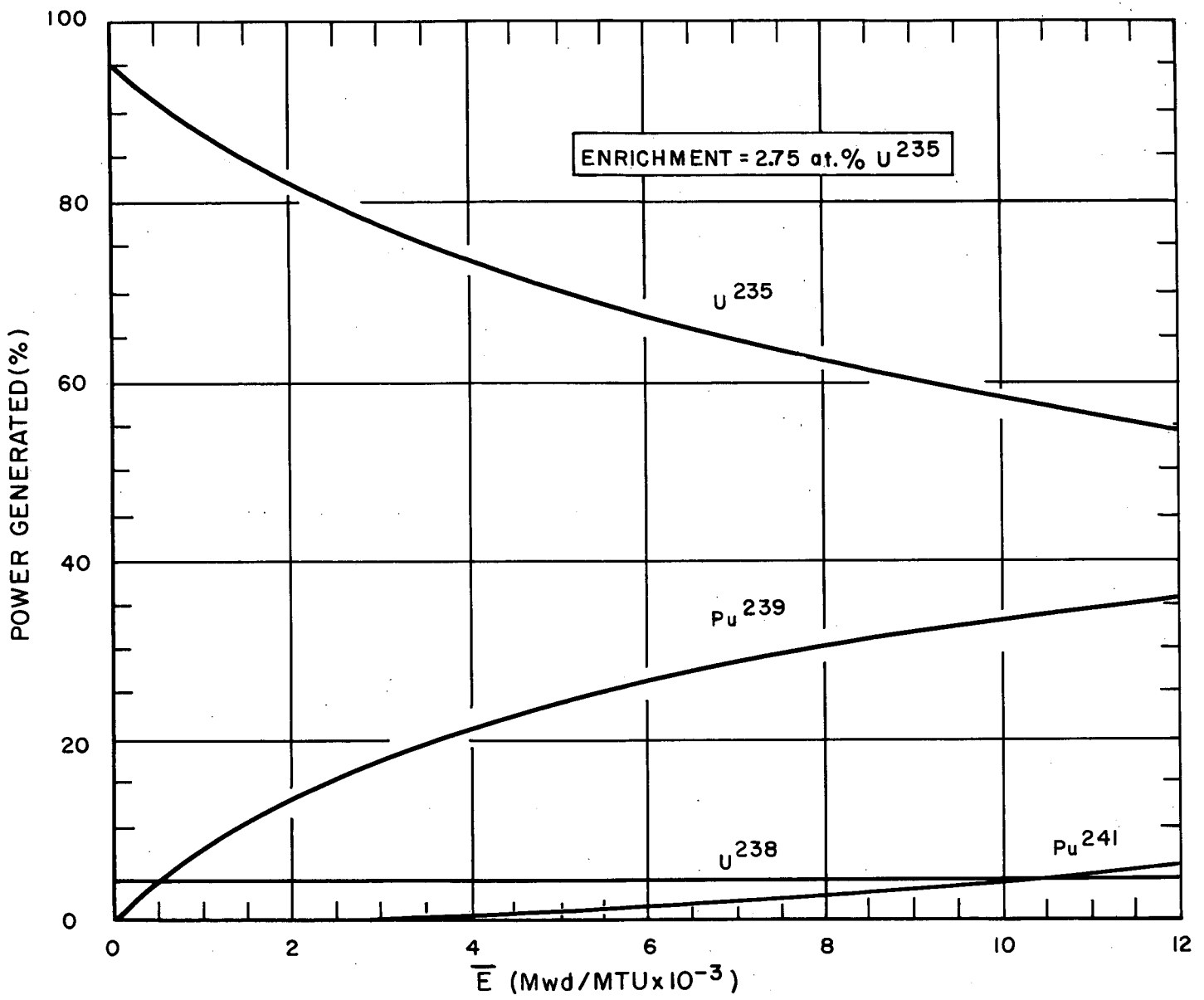

Figure 18B. Variation in Percentage of Total Power Generated by Each Fissionable Isotope as a Function of Burnup, 2.75 at. % U^{235} Enrichment

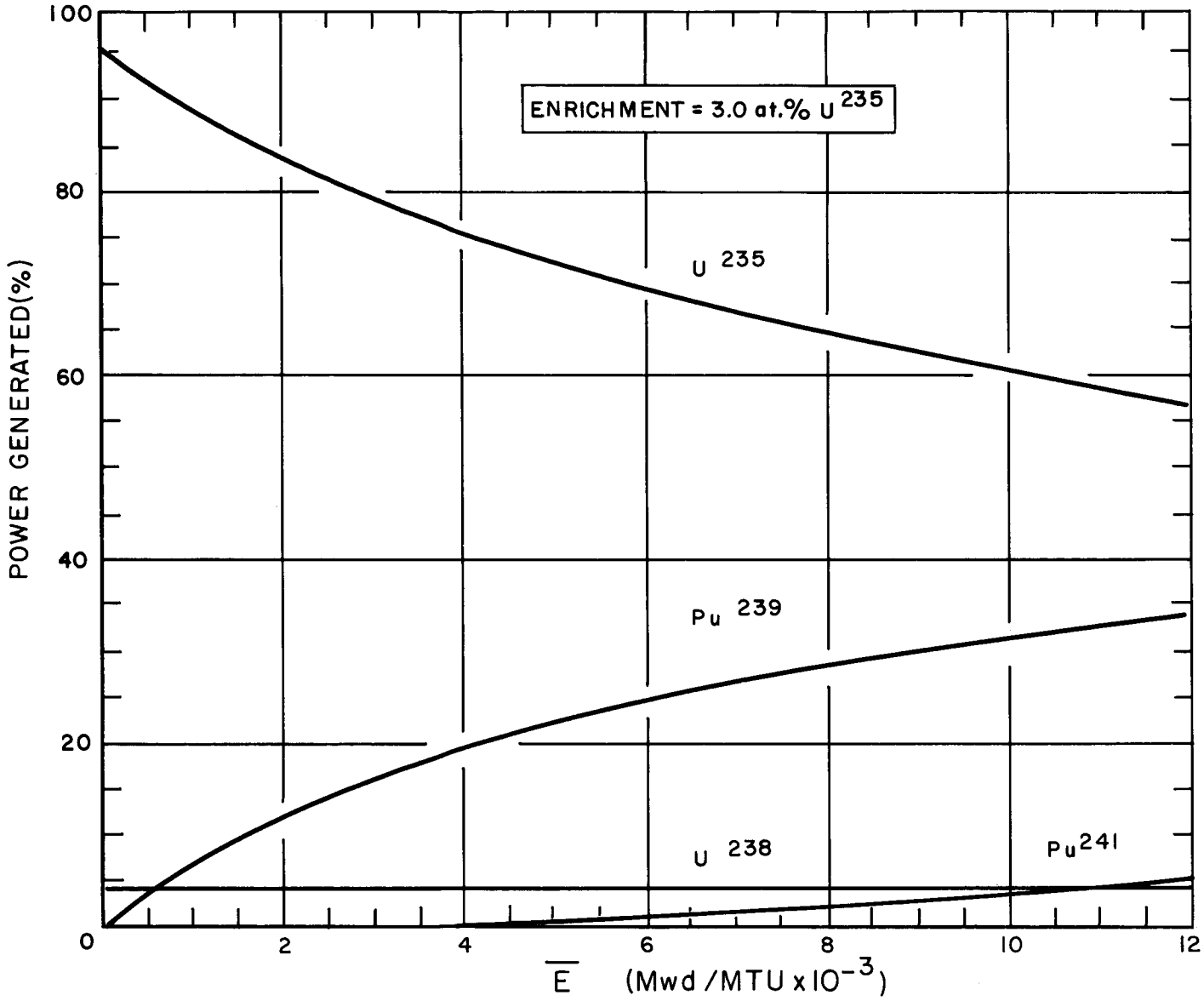

Figure 18C. Variation in Percentage of Total Power Generated by Each Fissionable Isotope as a Function of Burnup, 3.0 at. % U^{235} Enrichment

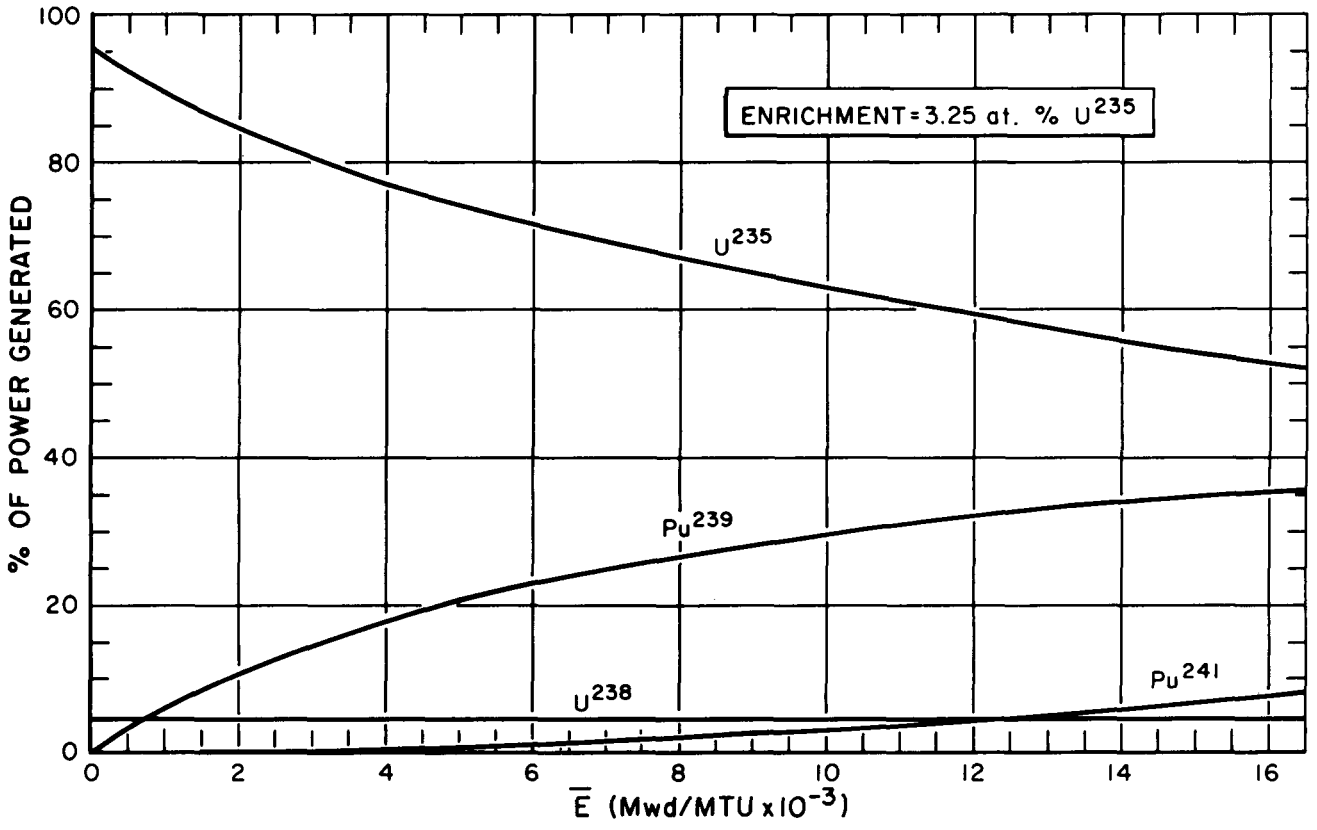

Figure 18D. Variation in Percentage of Total Power Generated by Each Fissionable Isotope as a Function of Burnup, 3.25 at. % U^{235} Enrichment

Xe^{135} continues to be formed at a high rate from the decay of I^{135}, though it is not removed as rapidly. After a time the Xe^{135} concentration does decrease, since the I^{135} is not regenerated as rapidly. Eventually a new equilibrium concentration of Xe^{135}, and a new equilibrium Xe^{135} poisoning, for the new power level, will be reached. Since the maximum xenon concentration, and therefore the maximum Xe^{135} effect on reactivity, may be much larger at some time after a power reduction than it is under equilibrium conditions, it is necessary that there be sufficient excess reactivity available to over-ride the peak Xe^{135} poisoning after an anticipated power reduction, in order to be able to continue operation. If there is not sufficient excess reactivity available, a power reduction may cause a sufficient increase in poisoning to shut the reactor down completely. In this case it would be necessary to wait until the xenon concentration had decayed sufficiently to permit reactor startup.

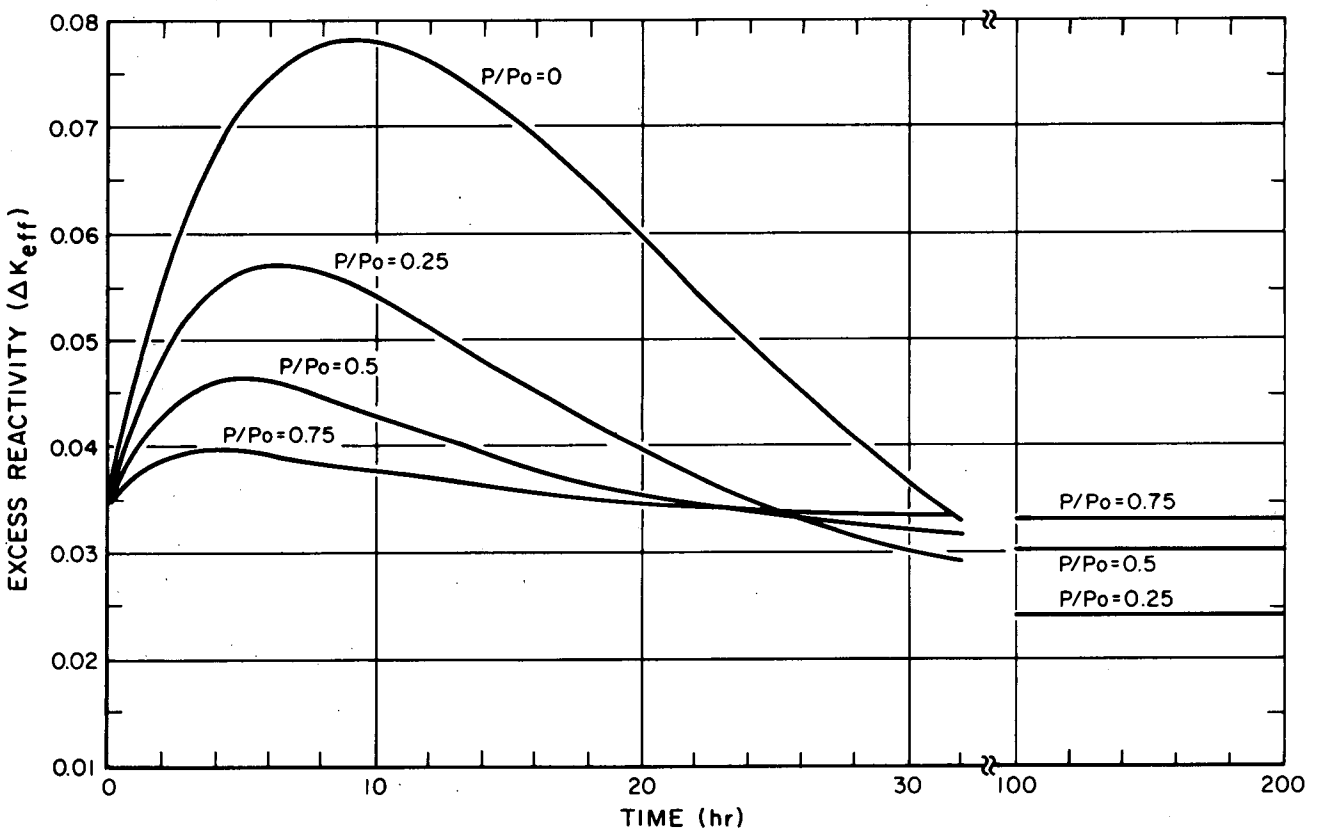

Figure 19. Decrease of Available Reactivity Due to Xenon Buildup After a Reduction in Power

APPENDIX I
USE OF GRAPHICAL RESULTS – TYPICAL CASE

The information presented in the preceding sections can be used to determine, for a given enrichment, what the predicted operational life of the core will be before a first refueling is required. The average exposure of the removed fuel can be estimated, and the uranium and plutonium content of the removed fuel can be obtained. An illustrative typical example follows.

If the reactor were originally loaded with 2.75 at. % U^{235} enriched fuel, the initial value of excess reactivity at full-power operation with equilibrium xenon and samarium poison present would be 0.104. This represents an idealized situation, since it is unlikely that the reactor would actually be loaded in all 150 fuel positions initially, if it resulted in this much excess reactivity. Instead there might be only a partial loading until the fuel elements had experienced sufficient exposure to reduce the excess reactivity to an acceptable level, at which time the rest of the core would be loaded. Alternatively, part of the core might be initially loaded with natural uranium elements to reduce the initial excess reactivity. For the purpose of this example, it will nevertheless be assumed that the core has been initially loaded in all 150 fuel positions with 2.75 at. % U^{235} enriched fuel.

It will be postulated that the operating condition which must be satisfied is that there shall be an excess of $\Delta k_{eff} = 0.02$ in the core at all times; i.e., when this condition no longer exists it will be necessary to partially reload the core with fresh fuel. Referring to Figure 19, it will be seen that this condition corresponds to the amount of excess reactivity necessary to over-ride, at any time, the peak xenon poisoning due to a power reduction of approximately 70%. From Figure 9 it is seen that in order for this condition to be satisfied, it will be necessary to reload fuel after an average core exposure of 9,350 Mwd/MTU.

If operation has been at an 80% plant load factor, the core has been in operation for 9,350 Mwd/MTU x 26.2 Days/1000 Mwd/MTU x 1/0.8 = 310 days.

The initial (hot-dirty) ratio of the peak radial power-generation rate to the average radial power-generation rate was 1.452, and, at 9,350 Mwd/MTU, it is 1.231 (Figure 13). The ratio of the radial peak fuel exposure to the average fuel exposure is 1.340 (Figure 12). The axial peak-to-average fuel exposure is 1.340,

and in a cluster the ratio is 1.072. This means that at an average core exposure of 9,350 Mwd/MTU, the peak fuel exposure is

$$9{,}350 \text{ Mwd/MTU} \times 1.340 \times 1.340 \times 1.072 = 18{,}000 \text{ Mwd/MTU}.$$

If, at this time, the reloading schedule calls for the reloading of half the core, the fuel is removed out to a radius of 123.5 cm. From Figure 14-B one can determine that the average exposure of the fuel removed is 11,000 Mwd/MTU. This result is obtained by interpolating between the curves for average core exposures of 9,000 and 12,000 Mwd/MTU. The peak radial exposure of the removed fuel is also determined from Figure 14-B as 12,500 Mwd/MTU, (the average exposure of the central fuel element) so that the ratio of average fuel exposure to peak radial fuel exposure in the removed fuel is 11,000 Mwd/MTU divided by 12,500 Mwd/MTU or 0.879. If there had been no self-flattening in the radial direction, the average-to-peak fuel exposure would have been .821 in the removed fuel.

From Figure 15-B, it is seen that the fuel initially contained 27.2 Kg U^{235}/MTU. In the fuel removed, there are 16.6 Kg U^{235}/MTU or a change in enrichment from 2.75 at. % U^{235} to 1.68 at. % U^{235}. There are 0.216 Kg of U^{236} formed for each Kg of U^{235} consumed. For the 10.60 Kg U^{235}/MTU that have been consumed in the removed fuel, there were 2.29 Kg/MTU of U^{236} formed and 8.31 Kg/MTU of U^{235} fissioned. In addition, there were 3.50 Kg/MTU of uranium fissioned as U^{238} or converted to plutonium and fissioned as Pu^{239} or Pu^{241}.

The plutonium content of the removed fuel can be seen in Figure 16-B. There are 2.70 Kg/MTU Pu^{239}, 1.08 Kg/MTU Pu^{240}, and 0.45 Kg/MTU of Pu^{241} for a total plutonium content of 4.23 Kg/MTU.

The average macroscopic thermal cross sections of the removed fuel are obtained from Figure 17-B. These are:

$$\Sigma_a/\Sigma_a(0) = 1.397$$
$$\Sigma_f/\Sigma_f(0) = 1.137$$
$$\nu\Sigma_f/\nu\Sigma_f(0) = 1.233.$$

At the beginning of core operation, 96% of the power was produced from fissions in U^{235} and 4% from fissions in U^{238}. At an average core exposure of 9,350 Mwd/MTU, 60% of the total power generated in the core was produced from fissions in U^{235}, 4.5% from fissions in U^{238}, 32% from fissions in Pu^{239}, and 3.5% from fissions in Pu^{241}. This is shown in Figure 18-B.

APPENDIX II
DISCUSSION OF THERMAL CROSS SECTIONS

The microscopic thermal neutron cross-sections used in this study are listed in Table II. These are based on the assumption of a Maxwellian distribution of thermal neutrons characterized by a neutron energy of 0.131 ev. (1250°C). The selection of cross section values is discussed in this Appendix.

Thermal scattering cross-sections were taken directly from values given in BNL 325, 2nd edition, wherever possible. It was assumed that they are independent of energy within the range of interest. Scattering cross sections for Pu^{240} and Pu^{241} were taken to be the same as for Pu^{239}. The value of 8.0 barns for U^{236} was estimated from the data given in BNL 325. Impurities in graphite were present in sufficiently small amounts to produce no effect on the scattering cross section. The scattering cross section for stainless steel is based on the value used by Fillmore.[7]

The 2200 m/s absorption cross-sections for most of the 1/v materials (carbon, sodium, zirconium, U^{236}, and U^{238}) were taken from BNL 325, 2nd edition. The value of absorption cross section for stainless steel was based on the value quoted by Fillmore.[7] The 2200-m/s cross-section for graphite was taken as 0.0053 barns, slightly higher than the value used by Fillmore, to make it representative of graphite grade currently being considered for SGR use.

The absorption cross section per average fission product pair was a matter of some uncertainty. Since the formulation to be used in the burnup study called for a single cross section to represent all the fission products, except for Xe^{135} and Sm^{149}, a decision was made to use the value quoted in the Nuclear Engineering Handbook.[9] This was treated as a 1/v absorber, and corrected to the proper neutron temperature.

For most of the non 1/v elements, the Maxwellian averaging was performed using the SOFOCATE Code.[10] Where values of Maxwellian-averaged cross sections were available from other sources for temperatures as high as 1250°C[12] or for lower temperatures,[13] they were compared with the values generated by SOFOCATE. A new source of Maxwellian-averaged cross sections for neutrons at 1250°C became available only after the work of this report had been substantially completed.[14]

The cross section for Xe^{135} was determined using SOFOCATE. The agreement was very good between the 2200 m/s value on which this is based, and the value from BNL-325. There is fair agreement, up to 837°C, the highest temperature for which Westcott has published values for Xe^{135}, between the values obtained from SOFOCATE and those obtained from Westcott's work. The value obtained from SOFOCATE is slightly higher than that from Westcott's work, but that is to be expected. The limit of integration in SOFOCATE is 0.625 ev, and in Westcott's work it is higher, thus making his data give more weight to the lower cross sections at higher energies.

For Sm^{149}, the Maxwellian averaging was interpolated from values obtained by Henderson.[12] The cross section is in good agreement with other data which became available subsequently.[14]

The Maxwellian averaging of U^{235} cross sections was done using SOFOCATE. The values obtained are slightly higher than those which would be obtained from Henderson's work, and higher still than those obtainable from Westcott's latest work. It seems possible to attribute the differences to the weight given to experimental data from various sources used in the integration.

The largest and most significant source of uncertainty lies in the plutonium cross sections. The existence of discrepancies between sets of Maxwellian-averaged Pu^{239} cross sections prepared from different sources has been recognized.[15] Since the capture-to-fission ratio increases in the 0.297 ev Pu^{239} resonance, the relative fission and absorption cross sections are strongly dependent on the neutron temperature and the limit to which the integration is carried. The Maxwellian-averaged cross sections for absorption and fission were computed using SOFOCATE and compared with Westcott's tabulations for temperatures up to 760°C, the highest temperature for which they were then available. There was good agreement between the values of $\overline{\sigma}_f$, predicted by both sources, up to 760°C. This gave some confidence to the values for higher energies generated by SOFOCATE, and the value for 1250°C was adapted. The values of $\overline{\sigma}_a$ generated by SOFOCATE were approximately 3.25% higher than the value from Westcott's tabulations, over the range for which a comparison was possible. The value calculated with SOFOCATE was arbitrarily reduced by this amount in order to bring it more into line with the capture-to-fission ratios predicted by Westcott.

The most recent tabulations extending to the temperatures used in this study[14] would lead to values of $\bar{\sigma}_a$ and $\bar{\sigma}_f$ significantly different than those used, though the capture-to-fission ratio is close. Conclusions regarding the relative plutonium isotope concentration and the fuel absorption cross section should be considered in this light.

For Pu^{240}, there is a considerable difference between the SOFOCATE code value of Maxwellian-averaged cross section that was used and that which is given by Westcott's recent tabulations. For temperatures up to 600°C, however, the agreement is good. The difference seems attributable to the presence of the 1.055 ev resonance. In the SOFOCATE work, the integration is carried out only to 0.625 ev and in the later Westcott work to 1.44 ev. The inclusion of this resonance in the Westcott averaging gives a much higher value for the Maxwellian average at 0.131 ev. In view of the group structure used for these studies, where the resonance region is treated separately, it appeared that the Maxwellian-averaged cross section from SOFOCATE was appropriate.

For Pu^{241}, the values from SOFOCATE were used, based on an absorption cross section at 2200 m/s normalized to 988 barns. The ratio of α - 1.365 was taken to be independent of energy. The values obtained in this way gave reasonable agreement with the recent Westcott tabulation.[14]

REFERENCES

1. G. L. Reed, "Evaluation of Calandria, Thimble and Canned Moderator Concepts for Sodium-Graphite Reactors," NAA-SR-3573 (to be published)

2. J. R. Churchill and J. Renard, "An Advanced Sodium Graphite Reactor Nuclear Power Plant," NAA-SR-3829 (to be published)

3. G. W. Stuart, "A Chart of Neutron Blackness for Solid Cylindrical Rods," HW-34187, (December 20, 1954)

4. R. R. McCready et al., "An IBM-704 Program for the Solution of the Neutron Transport Equation in Fifty Concentric Cylindrical Annuli by The Weil Method, Program 12," APEX-468 (September 1959)

5. O. J. Marlow et al., "WANDA" – A One-Dimensional Few-Group Diffusion Equation Code for the IBM-704," WAPD-TM-28 (November 1959)

6. H. Bohl, Jr., E. M. Gelbard, and G. H. Ryan, "MUFT-4 Fast Neutron Spectrum Code for the IBM-704," WAPD-TM-72, (July 1957)

7. F. L. Fillmore, "Two-Group Calculation of the Critical Core Size of the SRE Reactor," NAA-SR-1517 (Rev) (January 15, 1959)

8. S. Glasstone and M. C. Edlund, The Elements of Nuclear Reactor Theory, D. Van Nostrand, N. Y. 1952, p 235

9. H. Etherington (ed.) Nuclear Engineering Handbook, (1st ed. New York McGraw-Hill Book Company, Inc., 1955) p 2 to 11

10. H. Amster and R. Suarez, "A Calculation of Thermal Constants Averaged Over a Wigner-Wilkins Flux Spectrum: Description of the SOFOCATE Code," WAPD-TM-39, (January 1957)

11. O. J. Marlow and P. A. Ombrellaro, "CANDLE - A One-Dimensional Few-Group Depletion Code for the IBM-704," WAPD-TM-53, (May 1957)

12. W. B. Henderson and M. J. Stanley, "Cross Sections for Reactor Analysis," XDC 58-2-203, (1958)

13. C. H. Westcott, "Effective Cross Section Values for Well Moderated Thermal Reactor Spectra," CRRP-787 (Agusut 1, 1958)

14. C. H. Westcott and D. A. Roy, "Supplement to Effective Cross Section Values for Well Moderated Thermal Reactor Spectra," CRRP-862, (August 20, 1959)

15. T. J. Connolly, "Self-Sustaining Plutonium Recycle in Sodium Graphite Reactors," NAA-SR-3912, (September 1, 1959)

REFERENCES

16. T. J. Connolly, "Interm Report on Nuclear Analysis of SGR Fueling," NAA-SR-2561, (October 15, 1958)

17. O. R. Hillig, "Neutron Flux Distributions in a 19-Rod Fuel Element," (unpublished MS, Atomics International, Canoga Park, California, 1959)